Cocaine addiction-like behaviors are associated with long-term changes in gene regulation, energy metabolism, and GABAergic inhibition within the amygdala

Jessica L. Zhou[1,2], Giordano de Guglielmo[3], Aaron J. Ho[2], Marsida Kallupi[3], Hai-Ri Li[4], Apurva S. Chitre[3], Lieselot LG Carrette[3], Olivier George[3,4], Abraham A. Palmer[3,6], Graham McVicker[2*], Francesca Telese[3,4*]

[1]Bioinformatics and Systems Biology Program, University of California San Diego, La Jolla, CA, 92093, USA
[2]Integrative Biology Laboratory, Salk Institute for Biological Studies, 10010 N Torrey Pines Rd, La Jolla, CA, 92037, USA
[3]Department of Psychiatry, University of California, San Diego, La Jolla, CA, 92092, USA
[4]Department of Medicine, University of California San Diego, La Jolla, CA 92093, USA
[5]The Scripps Research Institute, 10550 N Torrey Pines Rd, La Jolla, CA, 92037, USA
[6]Institute for Genomic Medicine, University of California San Diego, 9500 Gilman Drive, La Jolla, CA 92093, USA

*Correspondence:
Francesca Telese (ftelese@ucsd.edu)
Graham McVicker (gmcvicker@salk.edu)

Abstract

The amygdala contributes to negative emotional states associated with relapse to drug seeking, but the cell type-specific gene regulatory programs that are involved in addiction are unknown. Here we generate an atlas of single nucleus gene expression and chromatin accessibility in the amygdala of outbred rats with low and high cocaine addiction-like behaviors following a prolonged period of abstinence. Between rats with different addiction indexes, there are thousands of cell type-specific differentially expressed genes and these are enriched for molecular pathways including GABAergic synapse in astrocytes, excitatory, and somatostatin neurons. We find that rats with higher addiction severity have excessive GABAergic inhibition in the amygdala, and that hyperpolarizing GABAergic transmission and relapse-like behavior are reversed by pharmacological manipulation of the metabolite methylglyoxal, a $GABA_A$ receptor agonist. By analyzing chromatin accessibility, we identify thousands of cell type-specific chromatin sites and transcription factor (TF) motifs where accessibility is associated with addiction-like behaviors, most notably at motifs for pioneer TFs in the FOX, SOX, and helix-loop-helix families.

Introduction

The amygdala mediates emotional processing of both rewarding and aversive environmental stimuli, which allows organisms to engage in subsequent valence-specific behaviors[1]. The amygdala is implicated in numerous neuropsychiatric disorders including addiction[2], and during excessive drug use, it regulates the negative emotions associated with drug withdrawal[3,4]. Avoidance of these negative emotions enhances the incentive value of the drug, leading to sustained drug-seeking behaviors and relapse[5–7]. Given prevention of relapse is the cornerstone of effective treatments for addiction, it is important to understand the amygdala's role in addiction and relapse.

The amygdala is composed of multiple discrete and interconnected subregions, each characterized by highly specialized neuronal populations distinguishable by their morphology and electrophysiological properties[8]. The major subdivisions include the basolateral amygdala (BLA), composed of excitatory glutamatergic neurons and inhibitory interneurons, and the central amygdala (CeA), composed of GABAergic neurons[9–11]. While the behavioral function and connectivity of individual subregions of the amygdala have recently been established[1], the mechanisms by which distinct subpopulations of neuronal and non-neuronal cells contribute to its function remains unclear.

Single-cell genomics is a powerful new approach for determining the cellular function and diversity of complex tissues like the amygdala. Single-cell RNA-sequencing (scRNA-seq), which profiles gene expression in individual cells, has identified and cataloged diverse cell types in human, mouse, and non-human primate brains[12–18]. In addition, single-cell assays for transposase-accessible chromatin (scATAC-seq), which profile open chromatin at single cell resolution, has identified regulatory DNA sequences in the rodent and human brain[12,19–25].

Regulatory elements identified by scATAC-seq include promoters and enhancers, which confer cell type-specificity to gene expression by recruiting sequence-specific transcription factors (TFs)[26–29].

Single cell assays have the potential to reveal, at a molecular level, how specialized amygdalar cell populations are involved in addiction. For example, given that most genetic variants associated with complex human diseases like addiction are located in noncoding regions of the genome[30], snATAC-seq could uncover genetically determined, cell-type specific differences and facilitate functional interpretation of genetic variants[31]. Thus far, however, the application of single-cell assays to the study of addiction-like behaviors in rodents has been limited. Single nucleus RNA-seq (snRNA-seq) has been applied to characterize cellular diversity in brain regions involved in the reward system[32–35], and has been used to analyze transcriptional changes induced by cocaine and morphine[36,37]. However, these prior studies used isogenic rodents, which means that genetically-mediated differences in susceptibility to addiction-like behaviors were not examined. Furthermore, these studies performed experiments following acute, experimenter-administration of drug treatments, which means that they reflect the acute effects of drug use rather than molecular differences associated with the development of long-lasting addictive-like behaviors. For these reasons, the results from prior single nucleus studies have significant limitations.

To address this knowledge gap, we performed snRNA-seq and snATAC-seq using amygdala tissue from outbred rats obtained from a large genetic study of cocaine addiction-related traits[38]. These rats are subjected to prolonged abstinence from voluntary cocaine intake in a well-validated model of extended access to drug intravenous self-administration (IVSA)[5,38–40]. IVSA is associated with neurochemical changes in key brain regions, which are similar to those observed in humans with cocaine use disorder[41]. This study used outbred heterogeneous stock (HS) rats because they have high levels of genetic variation and rich phenotypic diversity[42–45]. By analyzing differences in gene expression and chromatin accessibility in rats with low and high addiction indexes, we identify genes and transcriptional regulators associated with cocaine addiction-like behaviors, including those implicated in $GABA_A$ receptor-mediated pathways. Finally, we perform pharmacological manipulation in tissue slices and in rats to validate insights gained from the transcriptomic data.

Results

Behavioral characterization of HS rats exhibiting low or high cocaine addiction-like traits

To investigate how chronic cocaine use influences cellular states associated with addiction-like behaviors, we performed snRNA-seq and snATAC-seq on amygdala tissues from HS rats subjected to protracted abstinence (4 weeks) from extended access to cocaine IVSA[38,46–49] (Fig. 1a). The animals were trained to self-administer cocaine in operant chambers in two hour (short

access, ShA) and 6 hour (long access, LgA) sessions. We measured the mean number of cocaine rewards (lever presses) over the course of the behavioral protocol to quantify the escalation of intake, motivation (rewards measured in a progressive ratio (PR) schedule of reinforcement) and drug seeking despite adverse consequences (rewards paired with an electric foot-shock) (Fig. 1b). Based on individual behavioral measures (Fig. 1c), we calculated an addiction index (AI)[38] (average of the Z-score values of the three behavioral measures) as a measure of vulnerability (positive AI) or resilience (negative AI) to develop cocaine addiction-like behaviors. Based on the AI, we classified rats into high and low AI groups (Fig. 1d). High and low AI rats acquired different numbers of cocaine rewards during short access (ShA) vs long access (LgA) phases of the IVSA protocol (Fig. 1e, two-way repeated measures ANOVA, addiction index x phase interaction $p<0.0001$, $F_{23,1012}=8.523$). While there was no difference between groups in cocaine rewards during ShA sessions, high AI rats had a significantly higher escalation of drug intake during LgA sessions compared to low AI rats (Fig. 1e, $p<0.001$, post hoc comparisons with Bonferroni correction). We measured motivation with a PR schedule at the end of the ShA and LgA phases, where the number of lever presses required to acquire a cocaine infusion was increased progressively. Following extended access to cocaine self-administration, motivation for cocaine increased in the high AI rats but not in low AI rats (Fig. 1f, mixed effect model, addiction index × phase interaction, $p=0.0049$, $F_{1,41}=8.83$; Bonferroni corrected $p=0.0001$, post hoc comparisons). Finally, high AI rats showed increased responses despite adverse consequences compared to low AI rats, as demonstrated by the higher number of cocaine infusions when the reward was paired with an electric foot shock (Fig. 1g, $p<0.001$, unpaired t-test), which may reflect compulsive-like drug use. These results show that we can capture individual differences in multiple behavioral aspects that are relevant to cocaine use disorders by using the outbred population of HS rats in combination with the model of extended access to cocaine IVSA.

snRNA-seq and snATAC-seq defines distinct populations of cell types in the amygdala

The amygdala is thought to contribute to relapse through its regulation of negative emotional states associated with drug-seeking behavior. In rats, these negative emotional states progressively increase after withdrawal from drug IVSA[5,50]. To identify neuroadaptations that persist after chronic drug exposure during the withdrawal stage, we collected amygdala tissues after 4 weeks of abstinence from cocaine IVSA (Fig. 1a). We purified nuclei and measured the gene expression and open chromatin profiles of individual nuclei by performing snRNA-seq and snATAC-seq with the 10X Genomics Chromium workflow (see Methods). We performed these experiments on high and low AI rats, as well as naive rats (never exposed to cocaine). For snRNA-seq, we used 19 rats among which 6 were high AI, 6 were low AI, and 7 were naive. For snATAC-seq we used 12 rats among which 4 were high AI, 4 were low AI, and 4 were naive.

After filtering low quality nuclei and potential doublets based on quality metrics (Fig. S1-6, Table S1 and S2), we obtained a combined total of 163,003 and 81,912 high quality nuclei from the snRNA-seq and snATAC-seq experiments, respectively. Across the snRNA-seq samples, the mean reads per cell varied from 11,967 to 50,343 and the median number of detected genes

ranged from 1,293 to 2,855. Across the 12 snATAC-seq samples, the median number of high-quality fragments per nucleus ranged from 7,111 to 22,018. Using these data, we performed normalization, integration across rats, dimensionality reduction and clustering using Seurat[51] (snRNA) and Signac[52] (snATAC). In total, we identified 49 cell type clusters in the integrated snRNA-seq dataset and 41 cell type clusters in the integrated snATAC-seq dataset (Fig. S7). Visualization of the integrated data indicated that the clustering is not influenced by batch effects such as sequencing library, percentage of mitochondrial DNA, or individual rats[53] (Fig. S8).

We annotated the snRNA-seq clusters based on the expression of established cell type-specific marker genes[54–58] (Fig. 2a-b). The major cell types included excitatory neurons (denoted by expression of *Slc17a7)*, inhibitory GABAergic neurons (*Gad1/Gad2)*, astrocytes (*Gja1)*, microglia (*Ctss)*, mature oligodendrocytes (*Cnp)*, oligodendrocyte precursor cells (OPC) (*Pdgfra)*, and endothelial cells (*Cldn5)* (Fig. 2c). To annotate the snATAC-seq clusters, we estimated gene activity from pseudo bulk chromatin accessibility at promoter regions of cell marker genes and used these gene activity scores to impute gene expression in the snATAC-seq samples (Fig. S9). The imputed gene expression clearly delineates the cell clusters into the same major cell types described above demonstrating strong concordance between our snRNA-seq and snATAC-seq data (Fig. 2d). In addition to the major cell types, we also identified seven subtypes of inhibitory neurons based on the expression of known cell marker genes (Fig. 2e). We also sub-clustered the excitatory neurons and identified 18 distinct clusters (Fig. S10), with top markers including known subpopulation markers such as *Cdh13, Nr4a2, Bdnf*[59].

The total number of nuclei we obtained for each cell type varied substantially (Fig. 2f). As expected, excitatory and inhibitory neurons are the most common major cell types, with over 50,000 inhibitory neurons and 20,000 excitatory neurons in the snRNA-seq dataset. Endothelial cells and some subtypes of inhibitory and excitatory neurons have small numbers of nuclei in the dataset, so for most downstream analyses we focused on reporting the six most common major cell types (Fig. 2a-b).

In combination, the snRNA-seq and snATAC-seq datasets that we generated are the first single-cell atlas of molecularly-defined cell types in the rat amygdala. The inclusion of multiple high AI, low AI, and naive rats make these datasets an important resource for studying gene expression and chromatin accessibility in the amygdala under both normal conditions as well as in the context of cocaine addiction-like behaviors.

Measuring cell type-specific differential gene expression between rats displaying a high versus a low addiction index for cocaine

We used MAST[60], a generalized linear model designed for single-cell RNA-seq, to identify differentially expressed genes (DEGs) between high and low AI rats in each cell type(Fig. 3a-b, Table S3). To control for batch effects, which can cause false signals of differential expression in single cell data[61–63], we performed the same statistical test after permuting the AI labels of the rats. While the results from the unpermuted data are highly enriched for low p-values, the p-

values from the permuted data resemble the null expectation. This indicates that the DEGs we identified are unlikely to be caused by batch effects[61–63] (Fig. 3c, Fig. S11, Table S4).

We grouped DEGs into small (abs(avg_log_2FC)<0.1) or large effect size groups (abs(avg_log_2FC)≥0.1) and observed that most of the DEGs have small effect sizes (Fig. 3d). In total, we identified 1,227 unique DEGs with large effect sizes in at least one cell type and 13,114 DEGs with small effect sizes in at least one cell type. The number of significant DEGs (FDR<10%) between high and low AI rats correlates with the size of the cell type population, which likely reflects greater power to detect differential expression in common cell types (Fig. 3d). Most (1,078) of the large-effect DEGs are also a small-effect DEG in at least one other cell type, indicating that while there are shared patterns of differential expression across cell types, the effect sizes vary across cell types. We identified 65 DEGs with large effect sizes but discordant directions of effect across cell types (i.e. some genes that are substantially upregulated in one cell type are substantially downregulated in another). These results support our hypothesis that most addiction-related pathways operate via cell type-specific mechanisms (Fig. S12). Some of the most significant DEGs with the largest effect sizes have previously-reported roles in cocaine or other substance use disorders. Among these genes, *Ppp1r1b* (also known as dopamine- and cAMP-regulated phosphoprotein, 32 kDa, DARPP-32), is differentially expressed in both inhibitory neurons and astrocytes, and has long been associated with drugs of abuse[64–68]. Similarly, the proenkephalin encoding gene *Penk* is differentially expressed in Sst+ neurons and across different glial cell types and is associated with cocaine, opioid and cannabinoid use[69–71].

To identify pathways with altered regulation between high and low AI rats, we performed gene set enrichment analysis (GSEA)[72,73] to measure KEGG pathway enrichment in the cell type-specific DEGs. We identified significant enrichment of several pathways related to addiction (e.g. nicotine addiction and morphine addiction), neurotransmission (e.g. GABAergic, glutamatergic and dopaminergic synapse), stress (e.g. Cushing syndrome and cortisol synthesis), energy metabolism (e.g. glycolysis, pyruvate metabolism, and oxidative phosphorylation), and others (Fig. 3e, Table S5). Most cell types showed dysregulation of oxidative phosphorylation which, together with glucose metabolism, is the main energy source for synaptic activity and action potentials[74,75]. This observation suggests that addiction-like behaviors are associated with alterations in the metabolic state of amygdalar cell populations, which can directly impact neural network activity within the amygdala.

We closely examined the DEGs belonging to the GABAergic synapse pathway, which was significantly enriched in the DEGs of astrocytes, excitatory and Sst+ neurons (Fig. 3f) and found that genes involved in GABA type A ($GABA_A$) receptor signaling were more highly expressed in high versus low AI rats, including four $GABA_A$ receptors subunits (*Gabrg2, Gabrg3, Gabrb1, Gabra3*), four voltage-gated calcium channels (VGCCs) isoforms (*Cacan1a, Cacan1b, Cacan1c, Cacan1d*), and three protein kinase C (PKC) isoforms (*Prkca, Prkcb, Prkcg*). Long-term changes in $GABA_A$ receptor activity can be induced by signaling cascades, which are triggered by calcium influx through VGCCs and subsequent phosphorylation by PKC[3,76–78].

These results suggest that differences in $GABA_A$ receptor signaling in specific amygdalar cell types may be involved in cocaine addiction-related behaviors.

The development of cocaine addiction-like behaviors is linked to $GABA_A$ receptor-mediated hyperpolarizing inhibition in the amygdala

Based on the above results, we hypothesized that altered energy metabolism within the amygdala can alter $GABA_A$ receptor activity in the amygdala of high AI rats following prolonged abstinence from cocaine IVSA. To test this hypothesis, we measured GABAergic transmission by recording spontaneous inhibitory postsynaptic currents (sIPSCs) in the central amygdala (CeA). CeA slices were collected from a separate cohort of 5 low AI and 5 high AI HS rats that were subjected to prolonged abstinence following the same behavioral protocol described for the snRNA-seq and snATAC-seq experiments (Fig. 4a). As a control, we used CeA slices prepared from 5 age-matched naive HS rats to record baseline GABAergic transmission. There were significant differences in means among the groups (one-way ANOVA $F_{2,22}$=6.77, p=0.0051), and in post hoc tests, naive versus high AI rats were significantly different (Tukey HSD adjusted p-value=0.0037), reflecting an increase in GABAergic transmission from naive to low AI to high AI (Fig. 4b). These results suggest that the development of severe cocaine addiction-like behaviors coincides with a hyperpolarization of GABAergic transmission in the amygdala and are consistent with the results from our snRNA-seq differential gene expression analysis (Fig. 3a-b).

To further investigate the link between GABAergic transmission and energy metabolism in the amygdala with cocaine addiction-like behaviors, we modulated the activity of $GABA_A$ receptors by altering the endogenous levels of methylglyoxal (MG), which is a byproduct of glycolysis that has been shown to act as a competitive partial agonist of $GABA_A$ receptors[79]. To modulate MG levels in the amygdala, we inhibited glyoxalase 1 (GLO1), the rate limiting enzyme for the metabolism of MG, using S-bromobenzylglutathione cyclopentyl diester (pBBG)[79,80]. When we applied pBBG to CeA slices from naive, low AI or high AI rats, pBBG reduced the sIPSC frequency compared to vehicle for both high and low AI rats (paired t-tests, p=7.6e-5 and p=3.9e-3, respectively), but not naive rats (p=0.51) (Fig. 4c-f). These findings demonstrate that $GABA_A$ receptor-mediated hyperpolarization in high AI rats is normalized by the inhibition of GLO1.

These results led us to hypothesize that GLO1 inhibition would revert behavioral responses after prolonged abstinence from cocaine IVSA. To test this hypothesis, we measured cue-induced reinstatement of cocaine seeking behavior in a separate cohort of 26 low and high AI rats 30 minutes after systemic injection of pBBG or vehicle following 4 weeks of abstinence from cocaine IVSA (Fig. 4g). During this test, rats were subjected to the same operant conditions of cocaine IVSA, but without drug availability. Then, reinstatement was triggered by re-exposure to the cocaine infusion-associated light cue. The two-way repeated measures ANOVA showed a significant interaction between the addiction index and pharmacological treatment ($F_{1,24}$=6.609,

p<0.05), indicating that pBBG versus vehicle reduced cue-induced reinstatement in high AI rats (p-value<0.05, post hoc comparisons with Bonferroni correction), but not in low AI rats (p>0.05). Overall. these results demonstrate that modulating $GABA_A$ transmission with the pharmacological inhibition of GLO1 decreases relapse-like behaviors in animals with high cocaine AI.

Mapping differences in chromatin accessibility associated with to cocaine addiction-like behaviors

To identify regions of open chromatin from the snATAC-seq data, we used MACS2[81] to call accessible chromatin peaks from the aligned reads for each rat and created a union peak set across rats. We examined pseudo bulk chromatin accessibility at the TSS of selected cell type marker genes and observed cell type-specific patterns of accessibility at the expected marker genes of each cell type (Fig. 5a, Fig. 2c-d), indicating that the chromatin accessibility corresponds well with the transcriptome measurements.

Open chromatin regions harbor cell type-specific regulatory elements[82,83], and enrichment analyses that measure intersections between ATAC-seq peaks and GWAS signals can yield insight into the mechanisms by which genetic variants confer risk[84]. However, cell type-specific measurements of chromatin accessibility are difficult to obtain from human brain tissues. To assess whether our rat snATAC-seq data is meaningful for interpreting human addiction-related traits, we mapped the accessible chromatin peaks to the human reference genome and performed cell type-specific LD score regression[85]. We chose to use summary statistics from well-powered GWAS for alcohol and tobacco use[86,87] because there is significant genetic overlap among GWAS for all known substance use disorders[88] and because available GWAS for cocaine use disorder are much smaller and less powerful. We found significant enrichments (FDR<10%) of SNP heritability in every trait tested in almost every cell type (Fig. 5b), with the most significant enrichments in neurons, astrocytes, oligodendrocytes and OPCs. Overall, these results support the hypothesis that, despite the millions of years of evolution separating humans and rats, the regulatory architecture identified in HS rats that are divergent for IVSA-related phenotypes is relevant for human addiction-related traits.

To better understand the regulatory mechanisms involved in cocaine addiction, we analyzed differences in chromatin accessibility between high and low AI rats. We performed negative binomial tests to measure cell type-specific differential chromatin accessibility (Table S6), and compared the observed p-values to those obtained from permuted data (as we did for our DEG analysis). The p-values of the permuted data resemble the null expectation, confirming that the differential peaks between high and low addiction are likely true biological differences rather than batch effects (Fig. S13, Table S7). In total we identified >20,000 peaks across cell types with significant differential accessibility (FDR<10%), however, as with gene expression, most differences are small ($log_2FC < 0.1$) (Fig. S14). This indicates that differences in addiction-like behaviors between rats are associated with modest regulatory changes at a large number of sites.

The differential peaks can be subdivided into those where accessibility is higher (upregulated) or lower (downregulated) in the high AI rats (Fig. S14). In astrocytes, there are roughly equal numbers of up- and downregulated peaks, but the other cell types have profound biases. Excitatory neurons are the most biased with only two detected downregulated peaks, and over 8000 upregulated peaks. Inhibitory neurons show the opposite bias with over 4000 downregulated peaks but only ~500 upregulated peaks (Fig. S14). These biases likely reflect differences in the activity of specific TFs that control large transcriptional programs.

To determine whether the differential chromatin accessibility is consistent with the differential gene expression, we tested whether the promoters of DEGs are enriched for differential accessibility. We overlapped the significant differential accessible chromatin peaks in each cell type with the promoters of DEGs and computed a log odds ratio (log_2OR) as a measure of enrichment. Across all of the major cell types, there is a large and significant (Fisher's exact test, $p<0.05$) enrichment of differentially accessible peaks at the promoters of DEGs compared to non-DEGs (Fig. 5c, Table S8). This confirms that the differential chromatin accessibility and differential gene expression are concordant, and is additional evidence that the observed differences between high and low AI rats are true biological effects.

To characterize differentially accessible chromatin, we examined the genomic annotations for the significant differential peaks (Fig. S15). Differentially accessible peaks are highly enriched in promoter regions (compared to non-differential peaks), occurring there at least four times more frequently than expected in most of the major cell types (Fisher's exact test, FDR<10%) (Fig. 5d, Table S9). This enrichment may indicate that changes in chromatin are more concentrated at promoters, or that we have greater statistical power to detect changes at promoters, due to larger effect sizes or greater overall chromatin accessibility.

We hypothesized that differences in chromatin accessibility between high and low AI rats are caused by differential TF activity. To test this hypothesis, we analyzed the snATAC-seq data using chromVAR, which identifies TF motifs associated with differential accessibility using sparse single cell data[89]. A large number of motifs have significant differences in accessibility between the high and low AI rats, and since many TFs recognize similar motifs, we grouped them into motif clusters (see Methods) and summarized results across cell types (Fig. 5e).

The motif cluster with the most significant difference in accessibility between high and low AI rats contains motifs for basic helix-loop-helix (BHLH) TFs. This motif cluster has substantially higher accessibility within the excitatory neurons of high AI rats compared to low AI rats (deviance 3.8, p=1e-280), as well as a modest increase in accessibility in inhibitory neurons (deviance 0.38, p=1e-34) (Fig. 5f-h). The top-ranked motifs in this cluster all harbor the sequence CAGATGG, which is a close match to binding site motifs for multiple neuronal pioneer TFs including NeuroD1, NeuroD2, NeuroG2 and Atoh1[90,91]. Thus, the widespread increases in chromatin accessibility in excitatory neurons of high AI rats could reflect increased activity of pioneer TFs that recruit chromatin remodelers.

We noticed that many motif clusters with increased accessibility in the neurons of high AI rats have decreased accessibility in oligodendrocytes (Fig. 5e-h). Prominent among these motif clusters are those containing FOX and RFX motifs (Fig. 5e-h).

Several motif clusters also have opposite effects between excitatory and inhibitory neurons. SOX motifs have decreased accessibility in high AI rats in excitatory neurons but increased accessibility in all other major cell types including inhibitory neurons (Fig. 5e). MEF2 and FOS (AP1) motifs all have increased accessibility in the excitatory neurons of high AI rats but decreased accessibility in inhibitory neurons (Fig. 5e). AP1 and MEF2 motifs are of particular interest because they are associated with addiction[92–95] and their expression increases in the brain following chronic exposure to cocaine and other drugs[96–100].

While our analysis cannot pinpoint the precise TFs involved, it implicates many motif clusters that are associated with addiction-like behaviors across thousands of regulatory regions and in a cell type-specific manner.

Discussion

To better understand the molecular basis of addiction and illuminate long-term changes in gene regulation and chromatin accessibility associated with chronic drug use, we have generated an atlas of single-cell gene expression and chromatin accessibility in the amygdala of rats that showed divergent cocaine addiction-like behaviors. Our dataset is the largest resource of cell types in the mammalian amygdala, with over 163,000 nuclei in our snRNA-seq dataset and 81,000 nuclei in our snATAC-seq dataset (Fig. 2a-b). The snATAC-seq dataset provides the first map of cell type-specific regulatory elements in the amygdala, which has allowed us to identify TF motifs that may drive addiction-related processes.

Previous single cell transcriptomic studies have focused on the effects of acute passive treatment with psychoactive drugs in rodents[36,37], which cannot fully capture the motivational processes underlying addiction. In contrast, our behavioral protocol involves extended access to cocaine IVSA and reflects several key aspects of cocaine addiction, including escalation of drug use, enhanced motivation for drug seeking and taking, and persistent drug use despite adverse consequences, which might reflect compulsive-like drug consumption[101]. Thus, our study is the first to examine long-term molecular changes in distinct brain cell populations following abstinence from chronic voluntary cocaine use.

One striking finding from our study is that there are thousands of significant differences in gene expression and chromatin accessibility between high and low AI rats (Fig. 3d, Fig. S14). Most of these differences were small, which suggests that cocaine addiction-related behaviors may result from the combined action of many small effects on gene expression and chromatin accessibility. Because the HS rats are genetically diverse, the molecular differences between high and low AI rats could arise from genetic differences or from the consumption of different quantities of cocaine. These results are consistent with a polygenic model wherein addiction-like behaviors would result from the collective action of a large number of genetic risk loci with small

individual effects. This is a plausible explanation because of the high genetic diversity in the HS rats and because complex traits in humans are highly polygenic[102,103]. Further support for this hypothesis comes from DEGs such as *Pp1r1b* and *Penk* (Fig. 3a-b) which have gene expression quantitative trait loci (eQTLs) in HS rats[104], indicating that heritable differences influence their expression. Alternatively, the effects could be mediated by a relatively small number of TFs that affect many downstream genes and chromatin sites. Because some of the motifs with the strongest chromatin accessibility differences (Fig. 5e-h) are recognized by pioneer TFs (e.g. BHLH, SOX, FOX), it is tempting to speculate that widespread differences in accessibility are due to pioneer TFs, which have an intrinsic ability to modify chromatin[105]. These explanations are not mutually exclusive and it is likely that some differences are caused by eQTLs while others are caused by differences in the activity of upstream regulators (which themselves may be affected by genetics or other factors). To properly uncouple pre-existing genetically controlled gene expression differences from cocaine-induced neuroadaptations would require larger datasets of genotyped rats. One way this could be accomplished is through the use of polygenic risk scores for addiction-related traits, which will become possible as more rat behavioral GWAS are completed[42,44–46,106].

Human and animal studies have provided genetic and behavioral evidence that $GABA_A$ receptor-mediated pathways are involved in addiction[3,107–111]. Our differential gene expression (Fig. 3f) and electrophysiology (Fig. 4b) results support these prior findings and provide evidence for excessive GABAergic transmission in the high AI rats. Moreover, we found that inhibition of GLO1, the enzyme responsible for MG metabolism, normalizes electrophysiological (Fig. 4c-f) and behavioral differences (Fig. 4h) associated with severe addiction-like behaviors. While the pharmacological inhibition experiments are not cell type-specific, the transcriptomic data suggest that increases in GABAergic synapse-related genes may be specific to astrocytes, excitatory and Sst+ neurons. Furthermore, our results corroborate previous findings that MG acts as an endogenous competitive agonist for $GABA_A$ receptors[107,112], and offer a promising pharmacological target for improving therapeutic approaches for cocaine addiction. While our single-cell assays used only male rats, our validation experiments included both male and female rats. Future experiments including both sexes will be necessary to determine the influence of sex on gene expression and chromatin accessibility in the amygdala.

The results from the GLO1 inhibition experiments indicate a close connection between localized energy metabolism and neurotransmission[113]. Moreover, genes which are differentially regulated in high versus low AI rats are enriched in pathways related to energy metabolism, including glycolysis, pyruvate metabolism, and oxidative phosphorylation (Fig. 3e). Most notably, the expression levels of genes related to oxidative phosphorylation, which determines cellular ATP levels[114], are altered across most amygdalar cell types. Not only is ATP crucial for sustaining electrophysiological activity and cell signaling in the brain[115,116], but it is also required for ATP-dependent chromatin remodeling events initiated by pioneer TFs[117]. This could potentially explain why excitatory and inhibitory neurons show opposite directions of regulation in chromatin accessibility (Fig. S14) and in the enrichment of DEGs in the oxidative phosphorylation pathway (Fig. 3e). In combination, these observations suggest that an altered metabolic state within the amygdala impacts multiple cellular processes that are involved in

vulnerability to and development of addiction. Future experiments that directly manipulate the expression of specific metabolic enzymes or pioneer TFs in a cell type-specific manner will be necessary to fully elucidate their role in addiction.

In conclusion, the cellular atlas created by this study is a valuable resource for understanding cell type-specific gene regulatory programs in the amygdala and their role in the development of cocaine addiction-related behaviors. Our results emphasize the contribution of the $GABA_A$-mediated signaling to the enduring effects of cocaine use, which led us to perform experiments that manipulate $GABA_A$ transmission and identify a novel potential target for treatment of cocaine addiction. We anticipate that future studies will utilize our data to further investigate novel cell type-specific mechanisms involved in addiction.

Methods

Experimental

Animals

All protocols were reviewed and approved by the institutional Animal Care and Use Committee at the University of California San Diego. HS rats (Rat Genome Database NMcwiWFsm #13673907, sometimes referred to as N/NIH) which were created to encompass as much genetic diversity as possible at the NIH in the 1980's by outbreeding eight inbred rat strains (ACI/N, BN/SsN, BUF/N, F344/N, M520/N, MR/N, WKY/N and WN/N) were provided by Dr. Leah Solberg Woods (Wake Forest University School of Medicine). To minimize inbreeding and control genetic drift, the HS rat colony consists of more than 64 breeder pairs and is maintained using a randomized breeding strategy, with each breeder pair contributing one male and one female to subsequent generations. To keep track of the rats, their breeding, behavior, organs and genomic info, each rat received a chip with an RFID code. Rats were shipped at 3-4 weeks of age, kept in quarantine for 2 weeks and then housed two per cage on a 12 h/12 h reversed light/dark cycle in a temperature (20-22°C) and humidity (45-55%) controlled vivarium with ad libitum access to tap water and food pellets (PJ Noyes Company, Lancaster, NH, USA). We used 57 HS rats for the behavioral experiments, of which 31 male rats were used for the generation of genomic data and 26 rats (13 female, 13 male) were used for cue-induced reinstatement. For snRNA-seq we used 19 male rats (6 high AI, 6 low AI, 7 naive). For the snATAC-seq we used 12 male rats (4 high AI, 4 low AI, 4 naive). In addition, we used 15 female and male rats (5 high AI, 5 low AI, 5 naive) for the electrophysiology experiments.

Drugs

Cocaine HCl (National Institute on Drug Abuse, Bethesda, MD, USA) was dissolved in 0.9% saline (Hospira, Lake Forest, IL, USA) and administered intravenously at a dose of 0.5 mg/kg/infusion as described below. pBBG was synthesized in the laboratory of Prof. Dionicio Siegel (University of California San Diego, Skaggs School of Pharmacy and Pharmaceutical

Sciences). pBBG was dissolved in a vehicle of 8% dimethylsulfoxide, 18% Tween-80, and 74% distilled water and administered intraperitoneally 30 minutes before the test session.

Brain Samples

Brain tissues were obtained from the cocaine brain bank at UCSD[38], which collects tissues from HS rats that are part of an ongoing study of addiction-like behavior[42]. We used 31 HS rats for the generation of single-cell genomic data reported in this study which were selected as having low or high AI for cocaine addiction-related behaviors, using behavioral methods previously described[47]. Brain tissues were extracted and snap-frozen (at −30°C). Cryosections of approximately 500 microns (Bregma -1.80 - 3.30mm) were used to dissect the amygdala on a −20°C frozen stage, including the central nucleus of the amygdala, basolateral amygdala, and medial amygdala from both hemispheres. Punches from three sections were combined for each rat.

Single-cell library preparation, sequencing, and alignment

Single nucleus RNA-seq was performed by the Center for Epigenomics, UC San Diego using the Droplet-based Chromium Single-Cell 3' solution (10x Genomics, v3 chemistry). Briefly, frozen amygdala tissue was homogenized via glass dounce. Nuclei were then resuspended in 500 µL of nuclei permeabilization buffer (0.1% Triton-X-100 (Sigma-Aldrich, T8787), 1X protease inhibitor, 1 mM DTT, and 1U/µL RNase inhibitor (Promega, N211B), 2% BSA (Sigma-Aldrich, SRE0036) in PBS). Sample was incubated on a rotator for 5 min at 4°C and then centrifuged at 500 rcf for 5 min (4°C, run speed 3/3). Supernatant was removed and pellet was resuspended in 400 µL of sort buffer (1 mM EDTA 0.2 U/µL RNase inhibitor (Promega, N211B), 2% BSA (Sigma-Aldrich, SRE0036) in PBS) and stained with DRAQ7 (1:100; Cell Signaling, 7406). Up to 75,000 nuclei were sorted using a SH800 sorter (Sony) into 50 µL of collection buffer consisting of 1 U/µL RNase inhibitor in 5% BSA; the FACS gating strategy sorted based on particle size and DRAQ7 fluorescence. Sorted nuclei were then centrifuged at 1000 rcf for 15 min (4°C, run speed 3/3) and supernatant was removed. Nuclei were resuspended in 35 µL of reaction buffer (0.2 U/µL RNase inhibitor (Promega, N211B), 2% BSA (Sigma-Aldrich, SRE0036) in PBS) and counted on a hemocytometer. 12,000 nuclei were loaded onto a Chromium Controller (10x Genomics). Libraries were generated using the Chromium Single-Cell 3′ Library Construction Kit v3 (10x Genomics, 1000075) with the Chromium Single-Cell B Chip Kit (10x Genomics, 1000153) and the Chromium i7 Multiplex Kit for sample indexing (10x Genomics, 120262) according to manufacturer specifications. cDNA was amplified for 12 PCR cycles.

For snATAC-seq library preparations, nuclei were purified from frozen amygdala tissues using an established method[118]. Briefly, frozen amygdala tissue was homogenized using a 2 ml glass dounce with 1 ml cold 1x Homogenization Buffer (HB). The cell suspension was filtered using a 70 µm Flowmi strainer (BAH136800070, Millipore Sigma) and centrifuged at 350g for 5 min at 4°C. Nuclei were isolated by iodixanol (D1556, Millipore Sigma) density gradient. The nuclei iodixanol solution (25%) was layered on top of 40% and 30% iodixanol solutions. Samples were centrifuged in a swinging bucket centrifuge at 3,000g for 20 min at 4°C. Nuclei were isolated

from the 30-40% interface. Libraries were generated using the Chromium Next GEM Single Cell ATAC v1.1 (10x Genomics, PN-1000175) with the Chromium Next GEM Chip H Single Cell Kit (10x Genomics, 1000162) and the Chromium i7 Multiplex Kit for sample indexing (10x Genomics, 1000212) according to manufacturer specifications. DNA was amplified for 8 cycles. For both library types, SPRISelect reagent (Beckman Coulter, B23319) was used for size selection and clean-up steps. Final library concentration was assessed by Qubit dsDNA HS Assay Kit (Thermo-Fischer Scientific) and post library QC was performed using Tapestation High Sensitivity D1000 (Agilent) to ensure that fragment sizes were distributed as expected. Final libraries were sequenced using the NovaSeq6000 (Illumina).

Raw base call (BCL) files were used to generate FASTQ files using Cell Ranger 3.1.0 with the `cellranger mkfastq` command for RNA-seq reads and `cellranger-atac mkfastq` for ATAC-seq reads[119,120]. Next, we used `cellranger count` and `cellranger-atac count` to align the reads to a custom rat reference genome based on the UCSC rn6 reference genome[121–123]. This reference genome was created from FASTA and genome annotation files for Rattus norvegicus Rnor_6.0 (Ensembl release 98)[124] and JASPAR2022 motifs[125]. We then filtered cells based on quality control metrics and performed barcode and UMI counting for the RNA-seq and ATAC-seq reads.

Electrophysiology

Slices of the CeA were prepared from cocaine dependent rats during protracted abstinence or age-matched naive rats. High AI (n=5), low AI (n=5) and naive (n=5) rats were used for patch clamp baseline recordings. Slices from each group were also used to record iPSCs after pBBG treatment. The naive rats received sham IV surgery. The rats were deeply anesthetized with isoflurane and brains were rapidly removed and placed in oxygenated (95% O_2, 5% CO_2) ice-cold cutting solution that contained 206 mM sucrose, 2.5 mM KCl, 1.2 mM NaH_2PO_4, 7 mM $MgCl_2$, 0.5 mM $CaCl_2$, 26 mM $NaHCO_3$, 5 mM glucose, and 5 mM Hepes. Transverse slices (300 µm thick) were cut on a Vibratome (Leica VT1200S; Leica Microsystems) and transferred to oxygenated artificial cerebrospinal fluid (aCSF) that contained 130 mM NaCl, 2.5 mM KCl, 1.2 mM NaH_2PO_4, 2.0 mM $MgSO_4 \cdot 7H_2O$, 2.0 mM $CaCl_2$, 26 mM $NaHCO_3$, and 10 mM glucose. The slices were first incubated for 30 min at 35°C and then kept at room temperature for the remainder of the experiment. Individual slices containing CeA were transferred to a recording chamber that was mounted on the stage of an upright microscope (Olympus BX50WI). The slices were continuously perfused with oxygenated aCSF at a rate of 3 mL/min. Neurons were visualized with a 60Å~ water-immersion objective (Olympus), infrared differential interference contrast optics, and a charge coupled device camera (EXi Blue; QImaging). Whole-cell recordings were performed using a Multiclamp 700B amplifier (10-kHz sampling rate, 10-kHz low-pass filter) and Digidata 1440A and pClamp 10 software (Molecular Devices). Patch pipettes (4–6 MΩ) were pulled from borosilicate glass (Warner Instruments) and filled with 70 mM $KMeSO_4$, 55 mM KCl, 10 mM NaCl, 2 mM $MgCl_2$, 10 mM Hepes, 2 mM Na-ATP, and 0.2 mM Na-GTP. Pharmacologically isolated spontaneous inhibitory postsynaptic currents (sIPSCs) were recorded in the presence of the glutamate receptor blockers, CNQX (Tocris #0190) and APV (Tocris #189), and the GABA-B receptor antagonist CGP55845 (Tocris #1246). Experiments with a series resistance of >15 MΩ or >20% change in series resistance were

excluded from the final dataset. pBBG (2.5uM) was acutely applied in the bath. The frequency, amplitude, and kinetics of sIPSCs were analyzed using semi-automated threshold-based mini detection software (Easy Electrophysiology) and visually confirmed. Data were analyzed using Prism 9.0 software (GraphPad, San Diego, CA, USA) with one-way ANOVA followed by post hoc Tukey HSD test or with paired t-tests. The data are expressed as mean ± SEM unless otherwise specified. Values of $p < 0.05$ were considered statistically significant.

Behavioral experiments

Intravenous catheterization and behavioral testing of rats used for the generation of snRNA-seq and snATAC-seq were carried out using an established protocol of extended access to cocaine IVSA, PR testing, and foot shock, as reported previously[38,47,48]. Briefly, after surgical implantation of intravenous catheters and a week of recovery, HS rats were trained to self-administer cocaine (0.5 mg/kg/infusion) in 10 short access (ShA) sessions (2h/day, 5 days per week). Next, the animals were allowed to self-administer cocaine in 14 long access (LgA) sessions (6h/day, 5 days/week) to measure the escalation of drug intake. Following the escalation phase, rats were screened for motivation using the PR test and for persistent drug-seeking despite adverse consequences using contingent foot-shock. Rats were classified as having a low or high AI by a median split. AI was computed by averaging normalized measurements (z-scores) for the three behavioral tests (escalation, motivation, resistance to punishment)[126]. The z-scores are calculated as follows $z = \frac{x-\mu}{\sigma}$, where x is the raw value, μ is the mean of the cohort, and σ is the standard deviation of the cohort. Brain tissues were collected after four weeks of abstinence.

For the pBBG studies, rats were placed back in the self-administration chambers without the availability of cocaine 28 days after the last drug self-administration session and the number of responses to the previous drug-paired lever (cocaine seeking behavior) was measured 30 minutes after intraperitoneal injection of pBBG (15 mg/kg/ml) or its vehicle, in a Latin square design. Specifically, the rats were presented with a neutral stimulus (SN) in a 2 h session to control for the specificity of the discriminative stimulus (SD) in reinstating extinguished cocaine-seeking behavior. During the SN session, the illumination of a 2.8 W house light that is located at the top of the chamber's front panel served as a SN that signaled the non-availability of the reinforcer. Responses on the right, active lever were followed by 70-dB white noise, during which the lever remained inactive for 20 s. Two days later, the rats were presented with the SD. Reintroduction of the cocaine-related SD but not neutral cues significantly reinstated extinguished cocaine-seeking behavior that was measured as mean number of lever presses. Data were analyzed using Prism 9.0 software (GraphPad, San Diego, CA, USA). Self-administration data were analyzed using repeated-measures analysis of variance (ANOVA) or mixed effect model followed by Bonferroni post-hoc tests when appropriate. For pairwise comparisons, data were analyzed using the unpaired *t*-test. The data are expressed as mean ± SEM unless otherwise specified. Values of $p < 0.05$ were considered statistically significant.

Computational

Quality control and preprocessing of snRNA-seq data

All snRNA-seq preprocessing was performed with 10x Genomics Cell Ranger 3.1.0 and Seurat v3.2.3[51]. FASTQ files were aligned to the Rattus norvegicus Ensembl v98 reference genome (Rnor_6.0). For each sample, we loaded the filtered feature barcode matrices containing only detected cellular barcodes returned by `cellranger count` into Seurat. We computed the number of unique genes detected in each cell (nFeature_RNA); the total number of molecules detected within a cell (nCount_RNA); and the percentage of reads mapping to the mitochondrial genome (percent.mt) (Fig. S1-3, Table S1). We removed all cells for which the value of any of these metrics was more than three standard deviations from the mean within the sample ($x > \mu \pm 3\sigma$). Next, we normalized the count data for each sample using sctransform[127] with percent.mt as a covariate.

Integrating snRNA-seq data across samples and clustering

To integrate snRNA-seq data across all of our samples, we used reciprocal principal component analysis (RPCA), as implemented in Seurat[51,128]. First, we identified 2000 highly variable features (genes) across all of the samples to use as integration features using the `SelectIntegrationFeatures()` function, which we passed as anchor features (`anchor.features`) to the `PrepSCTIntegration()` function. Next, we performed dimensionality reduction with PCA on each sample using `RunPCA()`. After this, we ran the `FindIntegrationAnchors()` function to find a set of anchors between the list of Seurat objects from all of our samples using the same anchor features passed to `PrepSCTIntegration()`, specifying RPCA as the dimensional reduction method to be performed for finding anchors (`reduction = rpca`) and the first 30 RPCA dimensions to be used for specifying the k-nearest neighbor search space. Two rats (1 high AI, 1 low AI) were used as reference samples for the integration. We used the resulting anchor set to perform dataset integration across all of our samples using `IntegrateData()`. We clustered the integrated dataset by constructing a K-nearest neighbor (KNN) graph using the first 30 PCs followed by the Louvain algorithm, implemented in Seurat using the `FindNeighbors()` function followed by `FindClusters()`. Finally, we ran PCA once again on the integrated dataset and visualized the data using uniform manifold approximation and projection (UMAP). Visualization of the integrated data in two-dimensional space indicated that batch correction was successful (Fig. S8a-c).

Cell type assignment for snRNA-seq data

We identified marker genes of each cluster in our integrated snRNA-seq dataset using MAST[60], implemented with the `FindMarkers()` function in Seurat. Cell type identities were assigned based on expression of known marker genes of cell types known to be found in the amygdala.

Cell type-specific gene expression analysis for snRNA-seq data

Within each cell type, we tested for DEGs between the high AI rats and the low AI rats. We used MAST[60] implemented with the `FindMarkers()` function in Seurat to identify differential expression between groups, using percent.mt, the library prep date, and the rat sample ID as covariates. We did not pre-filter genes for testing based on log-fold change or minimum fraction of cells in which a gene was detected. This approach allowed us to detect weaker signals because we tested all observed genes in the dataset. Multiple testing correction was performed using the Benjamini-Hochberg method and we used a false discovery rate of 10% as a significance threshold (FDR<10%). Permutation tests were performed using the same methods, covariates, and filtering options but with shuffled addiction index labels and results were compared by visualizing the distributions of uncorrected p-values with QQ-plots (Fig. S11, Table S4). We used ClusterProfiler[129] to perform gene set enrichment analysis (GSEA) of KEGG pathways for DEGs from each cell type. Multiple testing correction for GSEA results was performed using Benjamini-Hochberg adjustment, with statistical significance assessed at a FDR<10%.

Per sample quality control and preprocessing of snATAC-seq data

As with the snRNA-seq data, we aligned the reads to the Rattus norvegicus Ensembl v98 reference genome (Rnor_6.0). All snATAC-seq data preprocessing was performed with MACS2[81] (for peak calling) and Signac[52]. Although peak calling is performed during alignment by `cellranger-atac count`, we chose to call peaks separately using MACS2 because Cell Ranger's peak calling function has been observed to merge multiple distinct peaks into a single region[130]. To minimize loss of informative features for clustering and downstream analysis, we first called peaks on the snATAC-seq BAM files for each rat with MACS2 (`macs2 callpeak -t {input} -f BAM -n {sample} --outdir {output} {params} --nomodel --shift -100 --ext 200 --qval 5e-2 -B --SPMR`). We confirmed that MACS2 calls more peaks and peaks with smaller widths compared to Cell Ranger (Fig. S16). Next, we merged overlapping peaks across all of our samples to generate a combined peak set using BEDtools[131] (`bedtools merge`). We generated a new peak by barcode matrix for each sample using this combined peak set and all detected cellular barcodes using the `FeatureMatrix()` function in Signac. We used these new matrices to create ChromatinAssay objects in Signac with the BSgenome.Rnorvegicus.UCSC.rn6[122] reference genome using the `CreateChromatinAssay()` function. From these ChromatinAssay objects we created Seurat objects with `CreateSeuratObject()`, which are compatible with functions from the Seurat package. We computed several quality control metrics for each sample: nucleosome banding pattern (nucleosome_signal); transcriptional start site (TSS) enrichment score (TSS.enrichment); total number of fragments in peaks (peak_region_fragments); and fraction of fragments in peaks (pct_reads_in_peaks) (Fig. S4-6, Table S2). We removed all cells for which the value of any of these metrics was more than two standard deviations from the mean within the sample ($x > \mu \pm 2\sigma$). We removed one rat (FTL_463_M757_933000320046135) from our dataset, due to the very low number of detected fragments per cell in this sample (Fig. S17).

Integrating snATAC-seq data across samples and clustering

Each sample was normalized using term frequency-inverse document frequency (TF-IDF) followed by singular value decomposition (SVD) on the TF-IDF matrix using all features (peaks)[52,130]. The combined steps of TF-IDF followed by SVD are known as latent semantic indexing (LSI)[132,133]. Non-linear dimensionality reduction and clustering were performed using UMAP and KNN following the same procedure used, respectively, just as we did for the snRNA-seq data. We merged the data across all samples within Signac and repeated the process of LSI in the same manner as it was applied to individual samples. We then integrated the merged dataset using Harmony[134] implemented by Signac, integrating over the sample library variable to account for the effects of different sequencing libraries used for different samples. We observed successful reduction of batch effects following integration Fig. S8d-f. We once again performed non-linear dimensionality reduction and clustering with UMAP and KNN, respectively. Notably, LSI, UMAP and KNN are used for visualization purposes; raw counts were used for downstream differential accessibility analyses.

Label transfer and cell type assignment for snATAC-seq data

We created a gene activity matrix for the integrated snATAC-seq data using the `GeneActivity()` function in Signac. This counts the number of fragments per cell overlapping the promoter region of a given gene and uses that value as a gene activity score. Gene activity serves as a proxy for gene expression as gene expression is often correlated with promoter accessibility. The gene activity scores were log normalized using the `NormalizeData()` function in Seurat with the normalization method set to `LogNormalize` and the scaling factor set to the median value of nCount_RNA across all cells, based on the gene activity scores. Cell type identities were assigned by integrating the snATAC-seq data with the integrated snRNA-seq data and performing label transfer[51] as described in Signac. Briefly, this approach identifies shared correlation patterns in the gene activity matrix and the scRNA-seq dataset to identify matched biological states across the two modalities. The process returns a classification score for each cell for each cell type defined in the scRNA-seq data. Each cell was assigned the cell type identity with the highest prediction score. Additionally, by identifying matched cells in the snRNA-seq dataset, we were able to impute RNA expression values for each of the cells in our snATAC-seq dataset. This enabled us to perform correlative analyses of chromatin accessibility and gene expression in later downstream analyses, as it produced a pseudo-multimodal dataset.

Differential chromatin accessibility analysis of snATAC-seq data

Similar to our differential analyses of the snRNA-seq data, we tested for differentially accessible genomic regions between nuclei from the high versus low AI rats within each cell type. We used the negative binomial test[127,135] implemented with the `FindMarkers()` function from Seurat to model the raw snATAC-seq count data using peak_region_fragments, library batch date, and rat sample ID as covariates. Multiple testing correction was performed using Benjamini-Hochberg adjustment and a false discovery rate below 10% (FDR<10%) was used to determine statistical significance. Permutation tests were performed in the same manner as for the differential gene

719 expression analyses (using the same statistical test and covariates with shuffled addiction index
720 labels).

721 Partitioned heritability analysis

722 We downloaded summary statistics for the Liu et al. 2019 GWAS of tobacco and alcohol use[86]
723 and used the munge_sumstats.py script from LD Score (LDSC)[102] to parse the summary
724 statistics file into the proper format for downstream analyses. We used the sets of significant
725 differential peaks (FDR<10%) for each cell type as foreground peaks and DNaseI
726 hypersensitivity profiles for 53 epigenomes from ENCODE Honeybadger2. We used the UCSC
727 liftOver tool to convert the foreground peaks from rn6 to hg19. There was no need to lift over the
728 background peaks as Honeybadger2 is already in hg19. Next, we generated partitioned LD
729 scores for the background and foreground regions. We used the make_annot.py script to make
730 annotation files and the ldsc.py script to compute annotation-specific LD scores. We used the
731 European 1000 Genomes Phase 3 PLINK[136] files to compute the LD scores. Finally, using the
732 baseline model and standard regression weights from the LDSC Partitioning Heritability tutorial,
733 we ran a cell type-specific partitioned heritability analysis with the LD scores we computed.

734 Annotation of open chromatin regions

735 Before performing any differential analyses, we first used the annotatePeaks.pl script from the
736 HOMER suite to annotate open chromatin regions and significant differential peaks (FDR<10%)
737 for each cell type in our integrated dataset[137]. For each cell type, we performed a Fisher's Exact
738 Test to measure the enrichment of genomic regions annotated as a promoter region within the
739 differential peaks compared to the set of all peaks in the dataset and observed significant
740 results for all cell types tested. Specifically, we compared the ratio of peaks annotated as
741 promoter regions to non-promoter regions in the significant differential peaks (FDR<10%)
742 versus all other peaks.

743 Fisher's Exact Tests

744 We first performed a Fisher's Exact Test to measure enrichment of DEGs (FDR<10%) with
745 differentially accessible promoters. We defined the latter as the case where the promoter region
746 of a gene overlaps a significant differentially accessible peak (FDR<10%). We obtained gene
747 coordinates from the TxDb.Rnorvegicus.UCSC.rn6.refGene annotation package and defined
748 promoter regions as being 1500 bases upstream and 500 bases downstream of the TSS
749 (`promoters(genes(TxDb.Rnorvegicus.UCSC.rn6.refGene), upstream = 1500, downstream =
750 500)`). We then generated a confusion matrix from the following four values: the number of
751 DEGs with differentially accessible promoters; the number of DEGs with non-differentially
752 accessible promoters; the number of non-DEGs with differentially accessible promoters; and the
753 number of non-DEGs with non-differentially accessible promoters. We then performed a
754 Fisher's Exact Test to measure enrichment of differentially accessible peaks (FDR<10%) which
755 were annotated as TSS/promoter regions by HOMER (annotatePeaks.pl). We generated a
756 confusion matrix from the following four values: the number of differential peaks with a
757 TSS/promoter annotation; the number of differential peaks without a TSS/promoter annotation;

the number of non-differential peaks (FDR>10%) with a TSS/promoter annotation; and the number of non-differential peaks (FDR>10%) without a TSS/promoter annotation.

Measuring differential activity of transcription factors with chromVAR

We measured cell type specific motif activities using chromVAR to test for per motif deviations in accessibility between nuclei from high versus low AI rats. Motif data was pulled from the JASPAR2020 database, and integrated with snATAC-seq data using the `AddMotifs()` function in Signac. After adding motifs to our snATAC-seq dataset, we ran chromVAR with the `RunChromVAR()` wrapper in Signac. Differential analysis of chromVAR deviation scores was performed using the Wilcoxon Rank-Sum test between high AI rats versus lowly addicted rats within each cell type. Differential testing was performed using Seurat's `FindMarkers()` function with the mean function set as `rowMeans()` to calculate average difference in deviation scores between groups. Multiple testing correction was performed using Benjamini-Hochberg adjustment and a false discovery rate below 10% (FDR<10%) was used to determine statistical significance. Motif clusters were defined using the provided cluster numbers from JASPAR's matrix clustering-results and the names of the clusters were annotated by hand based on the what TFs were present in each cluster.When selecting clusters to visualize, we retrieved the top 50 motifs (FDR<10%) per cell-type and highlighted their respective clusters. Volcano plots and heatmap data were generated using Plotly in Python. Hierarchical ordering of heatmap clusters was generated with Plotly's `figure_factory.create_dendrogram()` function, which wraps the `cluster.hierarchy.dendrogram()` function in SciPy.

Data availability

The following publicly available datasets were used:
Rattus norvegicus Ensembl v98 reference genome and genome assembly (Rnor_6.0); JASPAR2022 transcription factor binding profiles for vertebrates; ENCODE Honeybadger 2 ChIP-seq; 1000 Genomes European reference panel; Liu et al. 2019[86] GWAS for tobacco and nicotine addiction.

Acknowledgements

We thank S. Preissl from the UC San Diego School of Medicine Center for Epigenomics for technical assistance with the snRNA-seq library preparation. We thank J. Hightower for assistance with figures preparation. We thank P. Montilla-Perez, L. Maturin and P. Schweitzer for technical assistance with sample collection and equipment maintenance. We thank Leah C. Solberg Woods for HS rats breeding colony management. We thank P. Fiaux for his assistance with generating supplementary figures. This work was supported by the National Institutes of Health (NIH) (U01DA050239 to F.T.; F31DA056226 to J.L.Z.; U01DA043799 to O.G., P50DA037844 to A.A.P.). G.d.G. was supported by the Brain and Behavior Research Foundation 2020 Young Investigator Award, and M.K. by the TDRP (T31KT1859 UC) grant.

This publication includes data generated at the UC San Diego IGM Genomics Center utilizing an Illumina NovaSeq 6000 that was purchased with funding from the NIH (S10OD026929).

Contributions

F.T. designed and coordinated the study. G.M. designed the overall bioinformatics analysis flow. J.L.Z. conducted bioinformatic analysis and data interpretation with inputs from F.T., G.M., and A.A.P. A.J.H. conducted chromVAR analysis. O.G. and G.d.G. designed the behavioral protocol for cocaine IVSA. G.d.G. performed the behavioral experiments. M.K. performed the electrophysiological experiments. L.L.C. dissected the brain samples. H.L. performed snATAC-seq experiments. A.S.C. provided genotype data for exploratory analysis. J.L.Z., G.M. and F.T. wrote the manuscript with contributions from all authors.

References

1. Janak PH, Tye KM. From circuits to behaviour in the amygdala. Nature. 2015 Jan 15;517(7534):284–292. PMCID: PMC4565157
2. Schumann CM, Bauman MD, Amaral DG. Abnormal structure or function of the amygdala is a common component of neurodevelopmental disorders. Neuropsychologia. 2011 Mar;49(4):745–759. PMCID: PMC3060967
3. Roberto M, Gilpin NW, Siggins GR. The Central Amygdala and Alcohol: Role of γ-Aminobutyric Acid, Glutamate, and Neuropeptides. Cold Spring Harb Perspect Med. 2012 Dec;2(12):a012195. PMCID: PMC3543070
4. Buffalari DM, See RE. Amygdala Mechanisms of Pavlovian Psychostimulant Conditioning and Relapse. In: Self DW, Staley Gottschalk JK, editors. Behavioral Neuroscience of Drug Addiction [Internet]. Berlin, Heidelberg: Springer; 2010 [cited 2022 Aug 4]. p. 73–99. Available from: https://doi.org/10.1007/7854_2009_18
5. Pickens CL, Airavaara M, Theberge F, Fanous S, Hope BT, Shaham Y. Neurobiology of the incubation of drug craving. Trends Neurosci. 2011 Aug;34(8):411–420. PMCID: PMC3152666
6. Kalivas PW, Volkow ND. The Neural Basis of Addiction: A Pathology of Motivation and Choice. AJP. American Psychiatric Publishing; 2005 Aug;162(8):1403–1413.
7. Kilts CD, Schweitzer JB, Quinn CK, Gross RE, Faber TL, Muhammad F, Ely TD, Hoffman JM, Drexler KPG. Neural Activity Related to Drug Craving in Cocaine Addiction. Archives of General Psychiatry. 2001 Apr 1;58(4):334–341.
8. Aerts T, Seuntjens E. Novel Perspectives on the Development of the Amygdala in Rodents. Front Neuroanat. 2021 Dec 9;15:786679. PMCID: PMC8696165
9. Arrigucci R, Bushkin Y, Radford F, Lakehal K, Vir P, Pine R, Martin D, Sugarman J, Zhao Y, Yap GS, Lardizabal AA, Tyagi S, Gennaro ML. FISH-Flow, a protocol for the concurrent detection of mRNA and protein in single cells using fluorescence in situ hybridization and flow cytometry. Nat Protoc. 2017 Jun;12(6):1245–1260. PMCID: PMC5548662
10. Ehrlich I, Humeau Y, Grenier F, Ciocchi S, Herry C, Lüthi A. Amygdala Inhibitory Circuits and the Control of Fear Memory. Neuron. Elsevier; 2009 Jun 25;62(6):757–771. PMID: 19555645
11. Ciocchi S, Herry C, Grenier F, Wolff SBE, Letzkus JJ, Vlachos I, Ehrlich I, Sprengel R, Deisseroth K, Stadler MB, Müller C, Lüthi A. Encoding of conditioned fear in central amygdala inhibitory circuits. Nature. Nature Publishing Group; 2010 Nov;468(7321):277–282.
12. Yao Z, Liu H, Xie F, Fischer S, Adkins RS, Aldridge AI, Ament SA, Bartlett A, Behrens MM, Van den Berge K, Bertagnolli D, de Bézieux HR, Biancalani T, Booeshaghi AS, Bravo HC, Casper T, Colantuoni C, Crabtree J, Creasy H, Crichton K, Crow M, Dee N, Dougherty EL, Doyle WI, Dudoit S, Fang R, Felix V, Fong O, Giglio M, Goldy J, Hawrylycz M, Herb BR, Hertzano R, Hou X, Hu Q, Kancherla J, Kroll M, Lathia K, Li YE, Lucero JD, Luo C, Mahurkar A, McMillen D, Nadaf NM, Nery JR, Nguyen TN, Niu SY, Ntranos V, Orvis J, Osteen JK, Pham T, Pinto-Duarte A, Poirion O, Preissl S, Purdom E, Rimorin C, Risso D, Rivkin AC, Smith K, Street K, Sulc J, Svensson V, Tieu M, Torkelson A, Tung H, Vaishnav ED, Vanderburg CR, van Velthoven C, Wang X, White OR, Huang ZJ, Kharchenko PV, Pachter L, Ngai J, Regev A, Tasic B, Welch JD, Gillis J, Macosko EZ, Ren B, Ecker JR, Zeng H, Mukamel EA. A transcriptomic and epigenomic cell atlas of the mouse primary motor cortex. Nature. 2021;598(7879):103–110. PMCID: PMC8494649
13. Bakken TE, Jorstad NL, Hu Q, Lake BB, Tian W, Kalmbach BE, Crow M, Hodge RD, Krienen FM, Sorensen SA, Eggermont J, Yao Z, Aevermann BD, Aldridge AI, Bartlett A, Bertagnolli D, Casper T, Castanon RG, Crichton K, Daigle TL, Dalley R, Dee N, Dembrow

N, Diep D, Ding SL, Dong W, Fang R, Fischer S, Goldman M, Goldy J, Graybuck LT, Herb BR, Hou X, Kancherla J, Kroll M, Lathia K, van Lew B, Li YE, Liu CS, Liu H, Lucero JD, Mahurkar A, McMillen D, Miller JA, Moussa M, Nery JR, Nicovich PR, Niu SY, Orvis J, Osteen JK, Owen S, Palmer CR, Pham T, Plongthongkum N, Poirion O, Reed NM, Rimorin C, Rivkin A, Romanow WJ, Sedeño-Cortés AE, Siletti K, Somasundaram S, Sulc J, Tieu M, Torkelson A, Tung H, Wang X, Xie F, Yanny AM, Zhang R, Ament SA, Behrens MM, Bravo HC, Chun J, Dobin A, Gillis J, Hertzano R, Hof PR, Höllt T, Horwitz GD, Keene CD, Kharchenko PV, Ko AL, Lelieveldt BP, Luo C, Mukamel EA, Pinto-Duarte A, Preissl S, Regev A, Ren B, Scheuermann RH, Smith K, Spain WJ, White OR, Koch C, Hawrylycz M, Tasic B, Macosko EZ, McCarroll SA, Ting JT, Zeng H, Zhang K, Feng G, Ecker JR, Linnarsson S, Lein ES. Comparative cellular analysis of motor cortex in human, marmoset and mouse. Nature. 2021;598(7879):111–119. PMCID: PMC8494640

14. Scala F, Kobak D, Bernabucci M, Bernaerts Y, Cadwell CR, Castro JR, Hartmanis L, Jiang X, Laturnus S, Miranda E, Mulherkar S, Tan ZH, Yao Z, Zeng H, Sandberg R, Berens P, Tolias AS. Phenotypic variation of transcriptomic cell types in mouse motor cortex. Nature. 2021;598(7879):144–150. PMCID: PMC8113357
15. Booeshaghi AS, Yao Z, van Velthoven C, Smith K, Tasic B, Zeng H, Pachter L. Isoform cell-type specificity in the mouse primary motor cortex. Nature. 2021;598(7879):195–199. PMCID: PMC8494650
16. Kozareva V, Martin C, Osorno T, Rudolph S, Guo C, Vanderburg C, Nadaf N, Regev A, Regehr WG, Macosko E. Author Correction: A transcriptomic atlas of mouse cerebellar cortex comprehensively defines cell types. Nature. 2022;602(7896):E21. PMCID: PMC8828463
17. Bhaduri A, Sandoval-Espinosa C, Otero-Garcia M, Oh I, Yin R, Eze UC, Nowakowski TJ, Kriegstein AR. An atlas of cortical arealization identifies dynamic molecular signatures. Nature. 2021;598(7879):200–204. PMCID: PMC8494648
18. Berg J, Sorensen SA, Ting JT, Miller JA, Chartrand T, Buchin A, Bakken TE, Budzillo A, Dee N, Ding SL, Gouwens NW, Hodge RD, Kalmbach B, Lee C, Lee BR, Alfiler L, Baker K, Barkan E, Beller A, Berry K, Bertagnolli D, Bickley K, Bomben J, Braun T, Brouner K, Casper T, Chong P, Crichton K, Dalley R, de Frates R, Desta T, Lee SD, D'Orazi F, Dotson N, Egdorf T, Enstrom R, Farrell C, Feng D, Fong O, Furdan S, Galakhova AA, Gamlin C, Gary A, Glandon A, Goldy J, Gorham M, Goriounova NA, Gratiy S, Graybuck L, Gu H, Hadley K, Hansen N, Heistek TS, Henry AM, Heyer DB, Hill D, Hill C, Hupp M, Jarsky T, Kebede S, Keene L, Kim L, Kim MH, Kroll M, Latimer C, Levi BP, Link KE, Mallory M, Mann R, Marshall D, Maxwell M, McGraw M, McMillen D, Melief E, Mertens EJ, Mezei L, Mihut N, Mok S, Molnar G, Mukora A, Ng L, Ngo K, Nicovich PR, Nyhus J, Olah G, Oldre A, Omstead V, Ozsvar A, Park D, Peng H, Pham T, Pom CA, Potekhina L, Rajanbabu R, Ransford S, Reid D, Rimorin C, Ruiz A, Sandman D, Sulc J, Sunkin SM, Szafer A, Szemenyei V, Thomsen ER, Tieu M, Torkelson A, Trinh J, Tung H, Wakeman W, Waleboer F, Ward K, Wilbers R, Williams G, Yao Z, Yoon JG, Anastassiou C, Arkhipov A, Barzo P, Bernard A, Cobbs C, de Witt Hamer PC, Ellenbogen RG, Esposito L, Ferreira M, Gwinn RP, Hawrylycz MJ, Hof PR, Idema S, Jones AR, Keene CD, Ko AL, Murphy GJ, Ng L, Ojemann JG, Patel AP, Phillips JW, Silbergeld DL, Smith K, Tasic B, Yuste R, Segev I, de Kock CPJ, Mansvelder HD, Tamas G, Zeng H, Koch C, Lein ES. Author Correction: Human neocortical expansion involves glutamatergic neuron diversification. Nature. 2022;601(7893):E12. PMCID: PMC8770134
19. Di Bella DJ, Habibi E, Stickels RR, Scalia G, Brown J, Yadollahpour P, Yang SM, Abbate C, Biancalani T, Macosko EZ, Chen F, Regev A, Arlotta P. Molecular Logic of Cellular Diversification in the Mouse Cerebral Cortex. Nature. 2021 Jul;595(7868):554–559. PMCID: PMC9006333
20. Ziffra RS, Kim CN, Ross JM, Wilfert A, Turner TN, Haeussler M, Casella AM, Przytycki PF,

Keough KC, Shin D, Bogdanoff D, Kreimer A, Pollard KS, Ament SA, Eichler EE, Ahituv N, Nowakowski TJ. Single-cell epigenomics reveals mechanisms of human cortical development. Nature. 2021;598(7879):205–213. PMCID: PMC8494642

21. Zhang Z, Zhou J, Tan P, Pang Y, Rivkin AC, Kirchgessner MA, Williams E, Lee CT, Liu H, Franklin AD, Miyazaki PA, Bartlett A, Aldridge AI, Vu M, Boggeman L, Fitzpatrick C, Nery JR, Castanon RG, Rashid M, Jacobs MW, Ito-Cole T, O'Connor C, Pinto-Duartec A, Dominguez B, Smith JB, Niu SY, Lee KF, Jin X, Mukamel EA, Behrens MM, Ecker JR, Callaway EM. Epigenomic diversity of cortical projection neurons in the mouse brain. Nature. 2021;598(7879):167–173. PMCID: PMC8494636cek
22. Li YE, Preissl S, Hou X, Zhang Z, Zhang K, Qiu Y, Poirion OB, Li B, Chiou J, Liu H, Pinto-Duarte A, Kubo N, Yang X, Fang R, Wang X, Han JY, Lucero J, Yan Y, Miller M, Kuan S, Gorkin D, Gaulton KJ, Shen Y, Nunn M, Mukamel EA, Behrens MM, Ecker JR, Ren B. An atlas of gene regulatory elements in adult mouse cerebrum. Nature. 2021;598(7879):129–136. PMCID: PMC8494637
23. Liu H, Zhou J, Tian W, Luo C, Bartlett A, Aldridge A, Lucero J, Osteen JK, Nery JR, Chen H, Rivkin A, Castanon RG, Clock B, Li YE, Hou X, Poirion OB, Preissl S, Pinto-Duarte A, O'Connor C, Boggeman L, Fitzpatrick C, Nunn M, Mukamel EA, Zhang Z, Callaway EM, Ren B, Dixon JR, Behrens MM, Ecker JR. DNA methylation atlas of the mouse brain at single-cell resolution. Nature. 2021;598(7879):120–128. PMCID: PMC8494641
24. Domcke S, Hill AJ, Daza RM, Cao J, O'Day DR, Pliner HA, Aldinger KA, Pokholok D, Zhang F, Milbank JH, Zager MA, Glass IA, Steemers FJ, Doherty D, Trapnell C, Cusanovich DA, Shendure J. A human cell atlas of fetal chromatin accessibility. Science. 2020 Nov 13;370(6518):eaba7612. PMCID: PMC7785298
25. Zhang K, Hocker JD, Miller M, Hou X, Chiou J, Poirion OB, Qiu Y, Li YE, Gaulton KJ, Wang A, Preissl S, Ren B. A single-cell atlas of chromatin accessibility in the human genome. Cell. 2021 Nov 24;184(24):5985-6001.e19. PMCID: PMC8664161
26. Moore JE, Purcaro MJ, Pratt HE, Epstein CB, Shoresh N, Adrian J, Kawli T, Davis CA, Dobin A, Kaul R, Halow J, Van Nostrand EL, Freese P, Gorkin DU, Shen Y, He Y, Mackiewicz M, Pauli-Behn F, Williams BA, Mortazavi A, Keller CA, Zhang XO, Elhajjajy SI, Huey J, Dickel DE, Snetkova V, Wei X, Wang X, Rivera-Mulia JC, Rozowsky J, Zhang J, Chhetri SB, Zhang J, Victorsen A, White KP, Visel A, Yeo GW, Burge CB, Lécuyer E, Gilbert DM, Dekker J, Rinn J, Mendenhall EM, Ecker JR, Kellis M, Klein RJ, Noble WS, Kundaje A, Guigó R, Farnham PJ, Cherry JM, Myers RM, Ren B, Graveley BR, Gerstein MB, Pennacchio LA, Snyder MP, Bernstein BE, Wold B, Hardison RC, Gingeras TR, Stamatoyannopoulos JA, Weng Z. Expanded encyclopaedias of DNA elements in the human and mouse genomes. Nature. 2020;583(7818):699–710. PMCID: PMC7410828
27. Shlyueva D, Stampfel G, Stark A. Transcriptional enhancers: from properties to genome-wide predictions. Nature Reviews Genetics. 2014 Apr;15(4):272–286.
28. Buenrostro JD, Wu B, Litzenburger UM, Ruff D, Gonzales ML, Snyder MP, Chang HY, Greenleaf WJ. Single-cell chromatin accessibility reveals principles of regulatory variation. Nature. 2015 Jul 23;523(7561):486–490. PMCID: PMC4685948
29. Cusanovich DA, Hill AJ, Aghamirzaie D, Daza RM, Pliner HA, Berletch JB, Filippova GN, Huang X, Christiansen L, DeWitt WS, Lee C, Regalado SG, Read DF, Steemers FJ, Disteche CM, Trapnell C, Shendure J. A Single-Cell Atlas of In Vivo Mammalian Chromatin Accessibility. Cell. Elsevier; 2018 Aug 23;174(5):1309-1324.e18. PMID: 30078704
30. Zhang F, Lupski JR. Non-coding genetic variants in human disease. Hum Mol Genet. 2015 Oct 15;24(R1):R102–R110. PMCID: PMC4572001
31. Srinivasan C, Phan BN, Lawler AJ, Ramamurthy E, Kleyman M, Brown AR, Kaplow IM, Wirthlin ME, Pfenning AR. Addiction-Associated Genetic Variants Implicate Brain Cell Type- and Region-Specific Cis-Regulatory Elements in Addiction Neurobiology. J Neurosci. 2021 Oct 27;41(43):9008–9030. PMCID: PMC8549541

32. Tran MN, Maynard KR, Spangler A, Huuki LA, Montgomery KD, Sadashivaiah V, Tippani M, Barry BK, Hancock DB, Hicks SC, Kleinman JE, Hyde TM, Collado-Torres L, Jaffe AE, Martinowich K. Single-nucleus transcriptome analysis reveals cell-type-specific molecular signatures across reward circuitry in the human brain. Neuron. Elsevier; 2021 Oct 6;109(19):3088-3103.e5. PMID: 34582785
33. Chen R, Blosser TR, Djekidel MN, Hao J, Bhattacherjee A, Chen W, Tuesta LM, Zhuang X, Zhang Y. Decoding molecular and cellular heterogeneity of mouse nucleus accumbens. Nat Neurosci. 2021 Dec;24(12):1757–1771. PMCID: PMC8639815
34. He J, Kleyman M, Chen J, Alikaya A, Rothenhoefer KM, Ozturk BE, Wirthlin M, Bostan AC, Fish K, Byrne LC, Pfenning AR, Stauffer WR. Transcriptional and anatomical diversity of medium spiny neurons in the primate striatum. Current Biology. Elsevier; 2021 Dec 20;31(24):5473-5486.e6. PMID: 34727523
35. Phillips RA, Tuscher JJ, Black SL, Andraka E, Fitzgerald ND, Ianov L, Day JJ. An atlas of transcriptionally defined cell populations in the rat ventral tegmental area. Cell Reports [Internet]. Elsevier; 2022 Apr 5 [cited 2022 Aug 4];39(1). Available from: https://www.cell.com/cell-reports/abstract/S2211-1247(22)00364-3 PMID: 35385745
36. Avey D, Sankararaman S, Yim AKY, Barve R, Milbrandt J, Mitra RD. Single-Cell RNA-Seq Uncovers a Robust Transcriptional Response to Morphine by Glia. Cell Rep. 2018 Sep 25;24(13):3619-3629.e4. PMCID: PMC6357782
37. Savell KE, Tuscher JJ, Zipperly ME, Duke CG, Phillips RA, Bauman AJ, Thukral S, Sultan FA, Goska NA, Ianov L, Day JJ. A dopamine-induced gene expression signature regulates neuronal function and cocaine response. Science Advances. American Association for the Advancement of Science; 2020 Jun 1;6(26):eaba4221.
38. Carrette LLG, Guglielmo G de, Kallupi M, Maturin L, Brennan M, Boomhower B, Conlisk D, Sedighim S, Tieu L, Fannon MJ, Velarde N, Martinez AR, Kononoff J, Kimbrough A, Simpson S, Smith LC, Shankar K, Ramirez FJ, Chitre AS, Lin B, Polesskaya O, Woods LCS, Palmer AA, George O. The Cocaine and Oxycodone Biobanks, Two Repositories from Genetically Diverse and Behaviorally Characterized Rats for the Study of Addiction. eNeuro [Internet]. Society for Neuroscience; 2021 May 1 [cited 2021 Aug 2];8(3). Available from: https://www.eneuro.org/content/8/3/ENEURO.0033-21.2021 PMID: 33875455
39. Chen BT, Yau HJ, Hatch C, Kusumoto-Yoshida I, Cho SL, Hopf FW, Bonci A. Rescuing cocaine-induced prefrontal cortex hypoactivity prevents compulsive cocaine seeking. Nature. Nature Publishing Group; 2013 Apr;496(7445):359–362.
40. Cohen A, Koob GF, George O. Robust Escalation of Nicotine Intake with Extended Access to Nicotine Self-Administration and Intermittent Periods of Abstinence. Neuropsychopharmacology. Nature Publishing Group; 2012 Aug;37(9):2153–2160.
41. Koob GF, Buck CL, Cohen A, Edwards S, Park PE, Schlosburg JE, Schmeichel B, Vendruscolo LF, Wade CL, Whitfield TW, George O. Addiction as a Stress Surfeit Disorder. Neuropharmacology. 2014 Jan;76(0 0):10.1016/j.neuropharm.2013.05.024. PMCID: PMC3830720
42. Solberg Woods LC, Palmer AA. Using Heterogeneous Stocks for Fine-Mapping Genetically Complex Traits. Methods Mol Biol. 2019;2018:233–247. PMCID: PMC9121584
43. Hansen C, Spuhler K. Development of the National Institutes of Health genetically heterogeneous rat stock. Alcohol Clin Exp Res. 1984 Oct;8(5):477–479. PMID: 6391259
44. Saar K, Beck A, Bihoreau MT, Birney E, Brocklebank D, Chen Y, Cuppen E, Demonchy S, Flicek P, Foglio M, Fujiyama A, Gut IG, Gauguier D, Guigo R, Guryev V, Heinig M, Hummel O, Jahn N, Klages S, Kren V, Kuhl H, Kuramoto T, Kuroki Y, Lechner D, Lee YA, Lopez-Bigas N, Lathrop GM, Mashimo T, Kube M, Mott R, Patone G, Perrier-Cornet JA, Platzer M, Pravenec M, Reinhardt R, Sakaki Y, Schilhabel M, Schulz H, Serikawa T, Shikhagaie M, Tatsumoto S, Taudien S, Toyoda A, Voigt B, Zelenika D, Zimdahl H, Hubner N. SNP and haplotype mapping for genetic analysis in the Rat. Nat Genet. 2008 May;40(5):560–566.

PMCID: PMC5915293
45. Baud A, Hermsen R, Guryev V, Stridh P, Graham D, McBride MW, Foroud T, Calderari S, Diez M, Ockinger J, Beyeen AD, Gillett A, Abdelmagid N, Guerreiro-Cacais AO, Jagodic M, Tuncel J, Norin U, Beattie E, Huynh N, Miller WH, Koller DL, Alam I, Falak S, Osborne-Pellegrin M, Martinez-Membrives E, Canete T, Blazquez G, Vicens-Costa E, Mont-Cardona C, Diaz-Moran S, Tobena A, Hummel O, Zelenika D, Saar K, Patone G, Bauerfeind A, Bihoreau MT, Heinig M, Lee YA, Rintisch C, Schulz H, Wheeler DA, Worley KC, Muzny DM, Gibbs RA, Lathrop M, Lansu N, Toonen P, Ruzius FP, de Bruijn E, Hauser H, Adams DJ, Keane T, Atanur SS, Aitman TJ, Flicek P, Malinauskas T, Jones EY, Ekman D, Lopez-Aumatell R, Dominiczak AF, Johannesson M, Holmdahl R, Olsson T, Gauguier D, Hubner N, Fernandez-Teruel A, Cuppen E, Mott R, Flint J. Combined sequence-based and genetic mapping analysis of complex traits in outbred rats. Nat Genet. 2013 Jul;45(7):10.1038/ng.2644. PMCID: PMC3821058
46. Carrette LLG, Corral C, Boomhower B, Brennan M, Crook C, Ortez C, Shankar K, Simpson S, Maturin L, Solberg Woods LC, Palmer AA, de Guglielmo G, George O. Leptin Protects Against the Development and Expression of Cocaine Addiction-Like Behavior in Heterogeneous Stock Rats. Front Behav Neurosci. 2022 Mar 3;16:832899. PMCID: PMC8934439
47. Characterization of cocaine addiction-like behavior in heterogeneous stock rats | bioRxiv [Internet]. [cited 2022 Jun 9]. Available from: https://www.biorxiv.org/content/10.1101/2021.07.22.453410v2
48. Sedighim S, Carrette LL, Venniro M, Shaham Y, de Guglielmo G, George O. Individual differences in addiction-like behaviors and choice between cocaine versus food in Heterogeneous Stock rats. Psychopharmacology (Berl). 2021 Dec;238(12):3423–3433. PMCID: PMC8889911
49. George O, Mandyam CD, Wee S, Koob GF. Extended Access to Cocaine Self-Administration Produces Long-Lasting Prefrontal Cortex-Dependent Working Memory Impairments. Neuropsychopharmacology. 2008 Sep;33(10):2474–2482. PMCID: PMC2760333
50. Koob GF, Volkow ND. Neurobiology of addiction: a neurocircuitry analysis. Lancet Psychiatry. 2016 Aug;3(8):760–773. PMCID: PMC6135092
51. Stuart T, Butler A, Hoffman P, Hafemeister C, Papalexi E, Mauck WM, Hao Y, Stoeckius M, Smibert P, Satija R. Comprehensive integration of single-cell data. Cell. 2019 Jun 13;177(7):1888-1902.e21. PMCID: PMC6687398
52. Stuart T, Srivastava A, Madad S, Lareau CA, Satija R. Single-cell chromatin state analysis with Signac. Nat Methods. Nature Publishing Group; 2021 Nov;18(11):1333–1341.
53. Butler A, Hoffman P, Smibert P, Papalexi E, Satija R. Integrating single-cell transcriptomic data across different conditions, technologies, and species. Nature Biotechnology. Nature Publishing Group; 2018 May;36(5):411–420.
54. Zeisel A, Hochgerner H, Lönnerberg P, Johnsson A, Memic F, van der Zwan J, Häring M, Braun E, Borm LE, La Manno G, Codeluppi S, Furlan A, Lee K, Skene N, Harris KD, Hjerling-Leffler J, Arenas E, Ernfors P, Marklund U, Linnarsson S. Molecular Architecture of the Mouse Nervous System. Cell. 2018 Aug 9;174(4):999-1014.e22. PMCID: PMC6086934
55. Saunders A, Macosko E, Wysoker A, Goldman M, Krienen F, de Rivera H, Bien E, Baum M, Wang S, Goeva A, Nemesh J, Kamitaki N, Brumbaugh S, Kulp D, McCarroll SA. Molecular Diversity and Specializations among the Cells of the Adult Mouse Brain. Cell. 2018 Aug 9;174(4):1015-1030.e16. PMCID: PMC6447408
56. Tasic B, Yao Z, Graybuck LT, Smith KA, Nguyen TN, Bertagnolli D, Goldy J, Garren E, Economo MN, Viswanathan S, Penn O, Bakken T, Menon V, Miller J, Fong O, Hirokawa KE, Lathia K, Rimorin christine, Tieu M, Larsen R, casper T, Barkan E, Kroll M, Parry S, Shapovalova NV, Hirschstein D, Pendergraft J, Sullivan HA, Kim TK, Szafer A, Dee N,

Groblewski P, Wickersham ian, cetin A, Harris JA, Levi BP, Sunkin SM, Madisen L, Daigle TL, Looger L, Bernard A, Phillips J, Lein E, Hawrylycz M, Svoboda K, Jones AR, Koch christof, Zeng H. Shared and distinct transcriptomic cell types across neocortical areas. Nature. 2018 Nov;563(7729):72–78. PMCID: PMC6456269

57. Yao Z, van Velthoven CTJ, Nguyen TN, Goldy J, Sedeno-Cortes AE, Baftizadeh F, Bertagnolli D, Casper T, Chiang M, Crichton K, Ding SL, Fong O, Garren E, Glandon A, Gouwens NW, Gray J, Graybuck LT, Hawrylycz MJ, Hirschstein D, Kroll M, Lathia K, Lee C, Levi B, McMillen D, Mok S, Pham T, Ren Q, Rimorin C, Shapovalova N, Sulc J, Sunkin SM, Tieu M, Torkelson A, Tung H, Ward K, Dee N, Smith KA, Tasic B, Zeng H. A taxonomy of transcriptomic cell types across the isocortex and hippocampal formation. Cell. 2021 Jun 10;184(12):3222-3241.e26. PMCID: PMC8195859
58. BRAIN Initiative Cell Census Network (BICCN). A multimodal cell census and atlas of the mammalian primary motor cortex. Nature. 2021 Oct;598(7879):86–102. PMCID: PMC8494634
59. O'Leary TP, Sullivan KE, Wang L, Clements J, Lemire AL, Cembrowski MS. Extensive and spatially variable within-cell-type heterogeneity across the basolateral amygdala. eLife. 9:e59003. PMCID: PMC7486123
60. Finak G, McDavid A, Yajima M, Deng J, Gersuk V, Shalek AK, Slichter CK, Miller HW, McElrath MJ, Prlic M, Linsley PS, Gottardo R. MAST: a flexible statistical framework for assessing transcriptional changes and characterizing heterogeneity in single-cell RNA sequencing data. Genome Biol [Internet]. 2015 [cited 2020 Oct 26];16. Available from: https://www.ncbi.nlm.nih.gov/pmc/articles/PMC4676162/ PMCID: PMC4676162
61. Leek JT, Scharpf RB, Bravo HC, Simcha D, Langmead B, Johnson WE, Geman D, Baggerly K, Irizarry RA. Tackling the widespread and critical impact of batch effects in high-throughput data. Nat Rev Genet. 2010 Oct;11(10):10.1038/nrg2825. PMCID: PMC3880143
62. Tran HTN, Ang KS, Chevrier M, Zhang X, Lee NYS, Goh M, Chen J. A benchmark of batch-effect correction methods for single-cell RNA sequencing data. Genome Biology. 2020 Jan 16;21(1):12.
63. Spielman RS, Bastone LA, Burdick JT, Morley M, Ewens WJ, Cheung VG. Common genetic variants account for differences in gene expression among ethnic groups. Nat Genet. 2007 Feb;39(2):226–231. PMCID: PMC3005333
64. Hamada M, Hendrick JP, Ryan GR, Kuroiwa M, Higashi H, Tanaka M, Nairn AC, Greengard P, Nishi A. Nicotine regulates DARPP-32 (dopamine- and cAMP-regulated phosphoprotein of 32 kDa) phosphorylation at multiple sites in neostriatal neurons. J Pharmacol Exp Ther. 2005 Nov;315(2):872–878. PMID: 16040813
65. Lee AM, Picciotto MR. Effects of nicotine on DARPP-32 and CaMKII signaling relevant to addiction. Adv Pharmacol. 2021;90:89–115. PMCID: PMC8008986
66. Nairn AC, Svenningsson P, Nishi A, Fisone G, Girault JA, Greengard P. The role of DARPP-32 in the actions of drugs of abuse. Neuropharmacology. 2004 Jan 1;47:14–23.
67. Zachariou V, Sgambato-Faure V, Sasaki T, Svenningsson P, Berton O, Fienberg AA, Nairn AC, Greengard P, Nestler EJ. Phosphorylation of DARPP-32 at Threonine-34 is required for cocaine action. Neuropsychopharmacology. 2006 Mar;31(3):555–562. PMID: 16123776
68. Zhu H, Lee M, Guan F, Agatsuma S, Scott D, Fabrizio K, Fienberg AA, Hiroi N. DARPP-32 phosphorylation opposes the behavioral effects of nicotine. Biol Psychiatry. 2005 Dec 15;58(12):981–989. PMID: 16084497
69. Jutras-Aswad D, Jacobs MM, Yiannoulos G, Roussos P, Bitsios P, Nomura Y, Liu X, Hurd YL. Cannabis-Dependence Risk Relates to Synergism between Neuroticism and Proenkephalin SNPs Associated with Amygdala Gene Expression: Case-Control Study. PLoS One. 2012 Jun 22;7(6):e39243. PMCID: PMC3382183
70. Moeller SJ, Beebe-Wang N, Schneider KE, Konova AB, Parvaz MA, Alia-Klein N, Hurd YL, Goldstein RZ. Effects of an opioid (proenkephalin) polymorphism on neural response to

errors in health and cocaine use disorder. Behav Brain Res. 2015 Oct 15;293:18–26. PMCID: PMC4567394

71. Nikoshkov A, Drakenberg K, Wang X, Horvath MCs, Keller E, Hurd YL. Opioid neuropeptide genotypes in relation to heroin abuse: Dopamine tone contributes to reversed mesolimbic proenkephalin expression. Proc Natl Acad Sci U S A. 2008 Jan 15;105(2):786–791. PMCID: PMC2206614
72. Subramanian A, Tamayo P, Mootha VK, Mukherjee S, Ebert BL, Gillette MA, Paulovich A, Pomeroy SL, Golub TR, Lander ES, Mesirov JP. Gene set enrichment analysis: A knowledge-based approach for interpreting genome-wide expression profiles. Proc Natl Acad Sci U S A. 2005 Oct 25;102(43):15545–15550. PMCID: PMC1239896
73. Mootha VK, Lindgren CM, Eriksson KF, Subramanian A, Sihag S, Lehar J, Puigserver P, Carlsson E, Ridderstråle M, Laurila E, Houstis N, Daly MJ, Patterson N, Mesirov JP, Golub TR, Tamayo P, Spiegelman B, Lander ES, Hirschhorn JN, Altshuler D, Groop LC. PGC-1α-responsive genes involved in oxidative phosphorylation are coordinately downregulated in human diabetes. Nat Genet. Nature Publishing Group; 2003 Jul;34(3):267–273.
74. Kasischke KA, Vishwasrao HD, Fisher PJ, Zipfel WR, Webb WW. Neural activity triggers neuronal oxidative metabolism followed by astrocytic glycolysis. Science. 2004 Jul 2;305(5680):99–103. PMID: 15232110
75. Attwell D, Laughlin SB. An energy budget for signaling in the grey matter of the brain. J Cereb Blood Flow Metab. 2001 Oct;21(10):1133–1145. PMID: 11598490
76. Lyons HR, Land MB, Gibbs TT, Farb DH. Distinct signal transduction pathways for GABA-induced GABA(A) receptor down-regulation and uncoupling in neuronal culture: a role for voltage-gated calcium channels. J Neurochem. 2001 Sep;78(5):1114–1126. PMID: 11553685
77. Brandon NJ, Jovanovic JN, Moss SJ. Multiple roles of protein kinases in the modulation of γ-aminobutyric acidA receptor function and cell surface expression. Pharmacology & Therapeutics. 2002 Apr 1;94(1):113–122.
78. Nakamura Y, Darnieder LM, Deeb TZ, Moss SJ. Regulation of GABAARs by Phosphorylation. Adv Pharmacol. 2015;72:97–146. PMCID: PMC5337123
79. Distler MG, Plant LD, Sokoloff G, Hawk AJ, Aneas I, Wuenschell GE, Termini J, Meredith SC, Nobrega MA, Palmer AA. Glyoxalase 1 increases anxiety by reducing GABAA receptor agonist methylglyoxal. J Clin Invest. 2012 Jun 1;122(6):2306–2315. PMCID: PMC3366407
80. Perez CL, Barkley-Levenson AM, Dick BL, Glatt PF, Martinez Y, Siegel D, Momper JD, Palmer AA, Cohen SM. A Metal-Binding Pharmacophore Library Yields the Discovery of a Glyoxalase 1 Inhibitor. J Med Chem. 2019 Feb 14;62(3):1609–1625. PMCID: PMC6467756
81. Zhang Y, Liu T, Meyer CA, Eeckhoute J, Johnson DS, Bernstein BE, Nusbaum C, Myers RM, Brown M, Li W, Liu XS. Model-based Analysis of ChIP-Seq (MACS). Genome Biology. 2008 Sep 17;9(9):R137.
82. Klemm SL, Shipony Z, Greenleaf WJ. Chromatin accessibility and the regulatory epigenome. Nat Rev Genet. Nature Publishing Group; 2019 Apr;20(4):207–220.
83. Song L, Zhang Z, Grasfeder LL, Boyle AP, Giresi PG, Lee BK, Sheffield NC, Gräf S, Huss M, Keefe D, Liu Z, London D, McDaniell RM, Shibata Y, Showers KA, Simon JM, Vales T, Wang T, Winter D, Zhang Z, Clarke ND, Birney E, Iyer VR, Crawford GE, Lieb JD, Furey TS. Open chromatin defined by DNaseI and FAIRE identifies regulatory elements that shape cell-type identity. Genome Res. 2011 Oct;21(10):1757–1767. PMCID: PMC3202292
84. Cano-Gamez E, Trynka G. From GWAS to Function: Using Functional Genomics to Identify the Mechanisms Underlying Complex Diseases. Front Genet. 2020 May 13;11:424. PMCID: PMC7237642
85. Finucane HK, Bulik-Sullivan B, Gusev A, Trynka G, Reshef Y, Loh PR, Anttila V, Xu H, Zang C, Farh K, Ripke S, Day FR, Purcell S, Stahl E, Lindstrom S, Perry JRB, Okada Y, Raychaudhuri S, Daly MJ, Patterson N, Neale BM, Price AL. Partitioning heritability by

functional annotation using genome-wide association summary statistics. Nature Genetics. Nature Publishing Group; 2015 Nov;47(11):1228–1235.

86. Liu M, Jiang Y, Wedow R, Li Y, Brazel DM, Chen F, Datta G, Davila-Velderrain J, McGuire D, Tian C, Zhan X, Choquet H, Docherty AR, Faul JD, Foerster JR, Fritsche LG, Gabrielsen ME, Gordon SD, Haessler J, Hottenga JJ, Huang H, Jang SK, Jansen PR, Ling Y, Mägi R, Matoba N, McMahon G, Mulas A, Orrù V, Palviainen T, Pandit A, Reginsson GW, Skogholt AH, Smith JA, Taylor AE, Turman C, Willemsen G, Young H, Young KA, Zajac GJM, Zhao W, Zhou W, Bjornsdottir G, Boardman JD, Boehnke M, Boomsma DI, Chen C, Cucca F, Davies GE, Eaton CB, Ehringer MA, Esko T, Fiorillo E, Gillespie NA, Gudbjartsson DF, Haller T, Harris KM, Heath AC, Hewitt JK, Hickie IB, Hokanson JE, Hopfer CJ, Hunter DJ, Iacono WG, Johnson EO, Kamatani Y, Kardia SLR, Keller MC, Kellis M, Kooperberg C, Kraft P, Krauter KS, Laakso M, Lind PA, Loukola A, Lutz SM, Madden PAF, Martin NG, McGue M, McQueen MB, Medland SE, Metspalu A, Mohlke KL, Nielsen JB, Okada Y, Peters U, Polderman TJC, Posthuma D, Reiner AP, Rice JP, Rimm E, Rose RJ, Runarsdottir V, Stallings MC, Stančáková A, Stefansson H, Thai KK, Tindle HA, Tyrfingsson T, Wall TL, Weir DR, Weisner C, Whitfield JB, Winsvold BS, Yin J, Zuccolo L, Bierut LJ, Hveem K, Lee JJ, Munafò MR, Saccone NL, Willer CJ, Cornelis MC, David SP, Hinds DA, Jorgenson E, Kaprio J, Stitzel JA, Stefansson K, Thorgeirsson TE, Abecasis G, Liu DJ, Vrieze S. Association studies of up to 1.2 million individuals yield new insights into the genetic etiology of tobacco and alcohol use. Nature Genetics. Nature Publishing Group; 2019 Feb;51(2):237–244.

87. Polimanti R, Walters RK, Johnson EC, McClintick JN, Adkins AE, Adkins DE, Bacanu SA, Bierut LJ, Bigdeli TB, Brown S, Bucholz KK, Copeland WE, Costello EJ, Degenhardt L, Farrer LA, Foroud TM, Fox L, Goate AM, Grucza R, Hack LM, Hancock DB, Hartz SM, Heath AC, Hewitt JK, Hopfer CJ, Johnson EO, Kendler KS, Kranzler HR, Krauter K, Lai D, Madden PAF, Martin NG, Maes HH, Nelson EC, Peterson RE, Porjesz B, Riley BP, Saccone N, Stallings M, Wall TL, Webb BT, Wetherill L, Edenberg HJ, Agrawal A, Gelernter J. Leveraging genome-wide data to investigate differences between opioid use vs. opioid dependence in 41,176 individuals from the Psychiatric Genomics Consortium. Molecular Psychiatry. Nature Publishing Group; 2020 Aug;25(8):1673–1687.

88. Hatoum AS, Johnson EC, Colbert SMC, Polimanti R, Zhou H, Walters RK, Gelernter J, Edenberg HJ, Bogdan R, Agrawal A. The addiction risk factor: A unitary genetic vulnerability characterizes substance use disorders and their associations with common correlates. Neuropsychopharmacology. 2022 Sep;47(10):1739–1745. PMCID: PMC9372072

89. Schep AN, Wu B, Buenrostro JD, Greenleaf WJ. chromVAR: inferring transcription-factor-associated accessibility from single-cell epigenomic data. Nature Methods. Nature Publishing Group; 2017 Oct;14(10):975–978.

90. Matsuda T, Irie T, Katsurabayashi S, Hayashi Y, Nagai T, Hamazaki N, Adefuin AMD, Miura F, Ito T, Kimura H, Shirahige K, Takeda T, Iwasaki K, Imamura T, Nakashima K. Pioneer Factor NeuroD1 Rearranges Transcriptional and Epigenetic Profiles to Execute Microglia-Neuron Conversion. Neuron. Elsevier; 2019 Feb 6;101(3):472-485.e7. PMID: 30638745

91. Glahs A, Zinzen RP. Putting chromatin in its place: the pioneer factor NeuroD1 modulates chromatin state to drive cell fate decisions. EMBO J. 2016 Jan 4;35(1):1–3. PMCID: PMC4718001

92. Cruz FC, Rubio FJ, Hope BT. Using c-fos to study neuronal ensembles in corticostriatal circuitry of addiction. Brain Res. 2015 Dec 2;1628(0 0):157–173. PMCID: PMC4427550

93. Zhang Y, Crofton EJ, Li D, Lobo MK, Fan X, Nestler EJ, Green TA. Overexpression of DeltaFosB in nucleus accumbens mimics the protective addiction phenotype, but not the protective depression phenotype of environmental enrichment. Frontiers in Behavioral Neuroscience [Internet]. 2014 [cited 2022 Aug 4];8. Available from: https://www.frontiersin.org/articles/10.3389/fnbeh.2014.00297

94. Bali P, Kenny PJ. Transcriptional mechanisms of drug addiction. Dialogues Clin Neurosci. 2019 Dec;21(4):379–387. PMCID: PMC6952748
95. Walker DM, Cates HM, Loh YHE, Purushothaman I, Ramakrishnan A, Cahill KM, Lardner CK, Godino A, Kronman HG, Rabkin J, Lorsch ZS, Mews P, Doyle MA, Feng J, Labonté B, Koo JW, Bagot RC, Logan RW, Seney ML, Calipari ES, Shen L, Nestler EJ. Cocaine self-administration alters transcriptome-wide responses in the brain's reward circuitry. Biol Psychiatry. 2018 Dec 15;84(12):867–880. PMCID: PMC6202276
96. Nestler EJ, Barrot M, Self DW. ΔFosB: A sustained molecular switch for addiction. Proceedings of the National Academy of Sciences. 2001 Sep 25;98(20):11042–11046.
97. Hope BT, Nye HE, Kelz MB, Self DW, Iadarola MJ, Nakabeppu Y, Duman RS, Nestler EJ. Induction of a long-lasting AP-1 complex composed of altered Fos-like proteins in brain by chronic cocaine and other chronic treatments. Neuron. Elsevier; 1994 Nov 1;13(5):1235–1244. PMID: 7946359
98. Nye HE, Nestler EJ. Induction of chronic Fos-related antigens in rat brain by chronic morphine administration. Mol Pharmacol. American Society for Pharmacology and Experimental Therapeutics; 1996 Apr 1;49(4):636–645. PMID: 8609891
99. Nye HE, Hope BT, Kelz MB, Iadarola M, Nestler EJ. Pharmacological studies of the regulation of chronic FOS-related antigen induction by cocaine in the striatum and nucleus accumbens. J Pharmacol Exp Ther. American Society for Pharmacology and Experimental Therapeutics; 1995 Dec 1;275(3):1671–1680. PMID: 8531143
100. Moratalla R, Elibol B, Vallejo M, Graybiel AM. Network-Level Changes in Expression of Inducible Fos–Jun Proteins in the Striatum during Chronic Cocaine Treatment and Withdrawal. Neuron. Elsevier; 1996 Jul 1;17(1):147–156. PMID: 8755486
101. Wade CL, Vendruscolo LF, Schlosburg JE, Hernandez DO, Koob GF. Compulsive-Like Responding for Opioid Analgesics in Rats with Extended Access. Neuropsychopharmacology. 2015 Jan;40(2):421–428. PMCID: PMC4443956
102. Bulik-Sullivan BK, Loh PR, Finucane HK, Ripke S, Yang J, Patterson N, Daly MJ, Price AL, Neale BM. LD Score regression distinguishes confounding from polygenicity in genome-wide association studies. Nature Genetics. Nature Publishing Group; 2015 Mar;47(3):291–295.
103. Visscher PM, Yengo L, Cox NJ, Wray NR. Discovery and implications of polygenicity of common diseases. Science. American Association for the Advancement of Science; 2021 Sep 24;373(6562):1468–1473.
104. Munro D, Wang T, Chitre AS, Polesskaya O, Ehsan N, Gao J, Gusev A, Woods LCS, Saba LM, Chen H, Palmer AA, Mohammadi P. The regulatory landscape of multiple brain regions in outbred heterogeneous stock rats [Internet]. bioRxiv; 2022 [cited 2022 Aug 17]. p. 2022.04.07.487560. Available from: https://www.biorxiv.org/content/10.1101/2022.04.07.487560v1
105. Zaret KS. Pioneer Transcription Factors Initiating Gene Network Changes. Annu Rev Genet. 2020 Nov 23;54:367–385. PMCID: PMC7900943
106. Chitre AS, Polesskaya O, Holl K, Gao J, Cheng R, Bimschleger H, Martinez AG, George T, Gileta AF, Han W, Horvath A, Hughson A, Ishiwari K, King CP, Lamparelli A, Versaggi CL, Martin C, St. Pierre CL, Tripi JA, Wang T, Chen H, Flagel SB, Meyer P, Richards J, Robinson TE, Palmer AA, Woods LCS. Genome wide association study in 3,173 outbred rats identifies multiple loci for body weight, adiposity, and fasting glucose. Obesity (Silver Spring). 2020 Oct;28(10):1964–1973. PMCID: PMC7511439
107. Stephens DN, King SL, Lambert JJ, Belelli D, Duka T. GABAA receptor subtype involvement in addictive behaviour. Genes Brain Behav. 2017 Jan;16(1):149–184. PMID: 27539865
108. Koob GF, Nestler EJ. The neurobiology of drug addiction. J Neuropsychiatry Clin Neurosci. 1997;9(3):482–497. PMID: 9276849

109. Koob GF. A role for GABA mechanisms in the motivational effects of alcohol. Biochemical Pharmacology. 2004 Oct 15;68(8):1515–1525.
110. Dixon CI, Morris HV, Breen G, Desrivieres S, Jugurnauth S, Steiner RC, Vallada H, Guindalini C, Laranjeira R, Messas G, Rosahl TW, Atack JR, Peden DR, Belelli D, Lambert JJ, King SL, Schumann G, Stephens DN. Cocaine effects on mouse incentive-learning and human addiction are linked to α2 subunit-containing GABAA receptors. Proc Natl Acad Sci U S A. 2010 Feb 2;107(5):2289–2294. PMCID: PMC2836671
111. Augier E, Barbier E, Dulman RS, Licheri V, Augier G, Domi E, Barchiesi R, Farris S, Nätt D, Mayfield RD, Adermark L, Heilig M. A molecular mechanism for choosing alcohol over an alternative reward. Science. American Association for the Advancement of Science; 2018 Jun 22;360(6395):1321–1326.
112. McMurray KMJ, Ramaker MJ, Barkley-Levenson AM, Sidhu PS, Elkin P, Reddy MK, Guthrie ML, Cook JM, Rawal VH, Arnold LA, Dulawa SC, Palmer AA. Identification of a novel, fast acting GABAergic anti-depressant. Mol Psychiatry. 2018 Feb;23(2):384–391. PMCID: PMC5608625
113. Harris JJ, Jolivet R, Attwell D. Synaptic Energy Use and Supply. Neuron. 2012 Sep 6;75(5):762–777.
114. Boyer PD. What makes ATP synthase spin? Nature. Nature Publishing Group; 1999 Nov;402(6759):247–249.
115. Du F, Zhu XH, Zhang Y, Friedman M, Zhang N, Uğurbil K, Chen W. Tightly coupled brain activity and cerebral ATP metabolic rate. Proc Natl Acad Sci U S A. 2008 Apr 29;105(17):6409–6414. PMCID: PMC2359810
116. Erecińska M, Silver IA. ATP and Brain Function. J Cereb Blood Flow Metab. SAGE Publications Ltd STM; 1989 Feb 1;9(1):2–19.
117. Swinstead EE, Paakinaho V, Presman DM, Hager GL. Pioneer factors and ATP-dependent chromatin remodeling factors interact dynamically: A new perspective. Bioessays. 2016 Nov;38(11):1150–1157. PMCID: PMC6319265
118. Duttke SH, Montilla-Perez P, Chang MW, Li H, Chen H, Carrette LLG, Guglielmo G de, George O, Palmer AA, Benner C, Telese F. Glucocorticoid Receptor-Regulated Enhancers Play a Central Role in the Gene Regulatory Networks Underlying Drug Addiction. Frontiers in Neuroscience [Internet]. 2022 [cited 2022 Jul 22];16. Available from: https://www.frontiersin.org/articles/10.3389/fnins.2022.858427
119. Satpathy AT, Granja JM, Yost KE, Qi Y, Meschi F, McDermott GP, Olsen BN, Mumbach MR, Pierce SE, Corces MR, Shah P, Bell JC, Jhutty D, Nemec CM, Wang J, Wang L, Yin Y, Giresi PG, Chang ALS, Zheng GXY, Greenleaf WJ, Chang HY. Massively parallel single-cell chromatin landscapes of human immune cell development and intratumoral T cell exhaustion. Nat Biotechnol. Nature Publishing Group; 2019 Aug;37(8):925–936.
120. Zheng GXY, Terry JM, Belgrader P, Ryvkin P, Bent ZW, Wilson R, Ziraldo SB, Wheeler TD, McDermott GP, Zhu J, Gregory MT, Shuga J, Montesclaros L, Underwood JG, Masquelier DA, Nishimura SY, Schnall-Levin M, Wyatt PW, Hindson CM, Bharadwaj R, Wong A, Ness KD, Beppu LW, Deeg HJ, McFarland C, Loeb KR, Valente WJ, Ericson NG, Stevens EA, Radich JP, Mikkelsen TS, Hindson BJ, Bielas JH. Massively parallel digital transcriptional profiling of single cells. Nat Commun. Nature Publishing Group; 2017 Jan 16;8(1):14049.
121. Navarro Gonzalez J, Zweig AS, Speir ML, Schmelter D, Rosenbloom KR, Raney BJ, Powell CC, Nassar LR, Maulding ND, Lee CM, Lee BT, Hinrichs AS, Fyfe AC, Fernandes JD, Diekhans M, Clawson H, Casper J, Benet-Pagès A, Barber GP, Haussler D, Kuhn RM, Haeussler M, Kent WJ. The UCSC Genome Browser database: 2021 update. Nucleic Acids Research. 2021 Jan 8;49(D1):D1046–D1057.
122. Team TBD. BSgenome.Rnorvegicus.UCSC.rn6: Full genome sequences for Rattus norvegicus (UCSC version rn6). 2014.

123. Kent WJ, Sugnet CW, Furey TS, Roskin KM, Pringle TH, Zahler AM, Haussler and D. The Human Genome Browser at UCSC. Genome Res. 2002 Jun 1;12(6):996–1006.
124. Cunningham F, Allen JE, Allen J, Alvarez-Jarreta J, Amode MR, Armean IM, Austine-Orimoloye O, Azov AG, Barnes I, Bennett R, Berry A, Bhai J, Bignell A, Billis K, Boddu S, Brooks L, Charkhchi M, Cummins C, Da Rin Fioretto L, Davidson C, Dodiya K, Donaldson S, El Houdaigui B, El Naboulsi T, Fatima R, Giron CG, Genez T, Martinez JG, Guijarro-Clarke C, Gymer A, Hardy M, Hollis Z, Hourlier T, Hunt T, Juettemann T, Kaikala V, Kay M, Lavidas I, Le T, Lemos D, Marugán JC, Mohanan S, Mushtaq A, Naven M, Ogeh DN, Parker A, Parton A, Perry M, Piližota I, Prosovetskaia I, Sakthivel MP, Salam AIA, Schmitt BM, Schuilenburg H, Sheppard D, Pérez-Silva JG, Stark W, Steed E, Sutinen K, Sukumaran R, Sumathipala D, Suner MM, Szpak M, Thormann A, Tricomi FF, Urbina-Gómez D, Veidenberg A, Walsh TA, Walts B, Willhoft N, Winterbottom A, Wass E, Chakiachvili M, Flint B, Frankish A, Giorgetti S, Haggerty L, Hunt SE, IIsley GR, Loveland JE, Martin FJ, Moore B, Mudge JM, Muffato M, Perry E, Ruffier M, Tate J, Thybert D, Trevanion SJ, Dyer S, Harrison PW, Howe KL, Yates AD, Zerbino DR, Flicek P. Ensembl 2022. Nucleic Acids Research. 2022 Jan 7;50(D1):D988–D995.
125. Castro-Mondragon JA, Riudavets-Puig R, Rauluseviciute I, Berhanu Lemma R, Turchi L, Blanc-Mathieu R, Lucas J, Boddie P, Khan A, Manosalva Pérez N, Fornes O, Leung TY, Aguirre A, Hammal F, Schmelter D, Baranasic D, Ballester B, Sandelin A, Lenhard B, Vandepoele K, Wasserman WW, Parcy F, Mathelier A. JASPAR 2022: the 9th release of the open-access database of transcription factor binding profiles. Nucleic Acids Research. 2022 Jan 7;50(D1):D165–D173.
126. Guglielmo G de, Carrette LL, Kallupi M, Brennan M, Boomhower B, Maturin L, Conlisk D, Sedighim S, Tieu L, Fannon MJ, Martinez A, Velarde N, Kononoff J, Kimbrough A, Simpson S, Smith LC, Shankar K, Crook C, Avelar A, Schweitzer P, Woods LCS, Palmer AA, George O. Characterization of cocaine addiction-like behavior in heterogeneous stock rats [Internet]. bioRxiv; 2021 [cited 2022 Aug 19]. p. 2021.07.22.453410. Available from: https://www.biorxiv.org/content/10.1101/2021.07.22.453410v2
127. Hafemeister C, Satija R. Normalization and variance stabilization of single-cell RNA-seq data using regularized negative binomial regression. bioRxiv. Cold Spring Harbor Laboratory; 2019 Mar 18;576827.
128. Richards LM, Riverin M, Mohanraj S, Ayyadhury S, Croucher DC, Díaz-Mejía JJ, Coutinho FJ, Dirks PB, Pugh TJ. A comparison of data integration methods for single-cell RNA sequencing of cancer samples [Internet]. bioRxiv; 2021 [cited 2022 May 19]. p. 2021.08.04.453579. Available from: https://www.biorxiv.org/content/10.1101/2021.08.04.453579v1
129. Wu T, Hu E, Xu S, Chen M, Guo P, Dai Z, Feng T, Zhou L, Tang W, Zhan L, Fu X, Liu S, Bo X, Yu G. clusterProfiler 4.0: A universal enrichment tool for interpreting omics data. The Innovation. 2021 Aug 28;2(3):100141.
130. Stuart T, Srivastava A, Lareau C, Satija R. Multimodal single-cell chromatin analysis with Signac. bioRxiv. Cold Spring Harbor Laboratory; 2020 Nov 10;2020.11.09.373613.
131. Quinlan AR, Hall IM. BEDTools: a flexible suite of utilities for comparing genomic features. Bioinformatics. 2010 Mar 15;26(6):841–842.
132. Cusanovich DA, Daza R, Adey A, Pliner H, Christiansen L, Gunderson KL, Steemers FJ, Trapnell C, Shendure J. Multiplex Single Cell Profiling of Chromatin Accessibility by Combinatorial Cellular Indexing. Science. 2015 May 22;348(6237):910–914. PMCID: PMC4836442
133. Deerwester S, Dumais ST, Furnas GW, Landauer TK, Harshman R. Indexing by latent semantic analysis. Journal of the American Society for Information Science. 1990;41(6):391–407.
134. Korsunsky I, Millard N, Fan J, Slowikowski K, Zhang F, Wei K, Baglaenko Y, Brenner M,

Loh P ru, Raychaudhuri S. Fast, sensitive and accurate integration of single-cell data with Harmony. Nature Methods. Nature Publishing Group; 2019 Dec;16(12):1289–1296.

135. Yirga AA, Melesse SF, Mwambi HG, Ayele DG. Negative binomial mixed models for analyzing longitudinal CD4 count data. Sci Rep. Nature Publishing Group; 2020 Oct 7;10(1):16742.

136. Purcell S, Neale B, Todd-Brown K, Thomas L, Ferreira MAR, Bender D, Maller J, Sklar P, de Bakker PIW, Daly MJ, Sham PC. PLINK: A Tool Set for Whole-Genome Association and Population-Based Linkage Analyses. Am J Hum Genet. 2007 Sep;81(3):559–575. PMCID: PMC1950838

137. Heinz S, Benner C, Spann N, Bertolino E, Lin YC, Laslo P, Cheng JX, Murre C, Singh H, Glass CK. Simple combinations of lineage-determining transcription factors prime cis-regulatory elements required for macrophage and B cell identities. Mol Cell. 2010 May 28;38(4):576–589. PMCID: PMC2898526

Figure 1

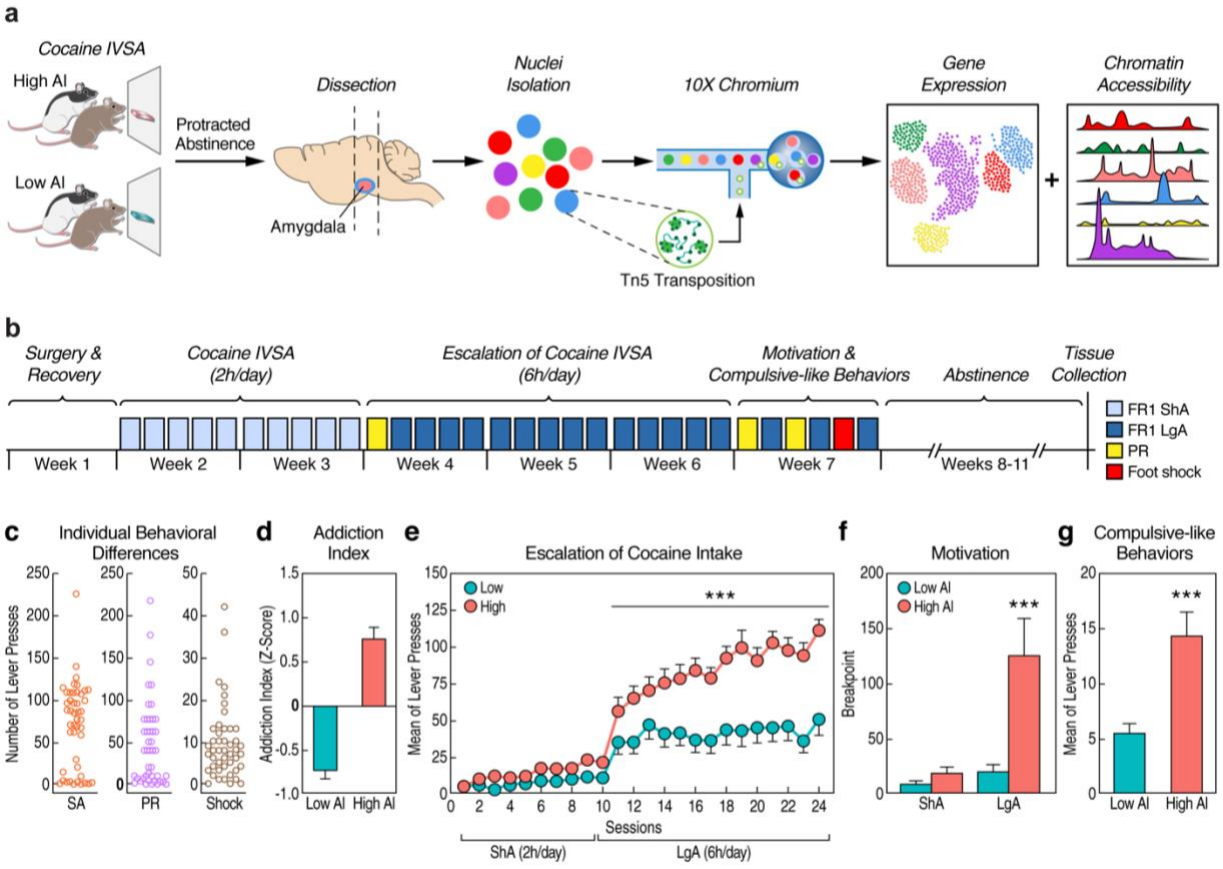

Figure 1. Experimental design and rat IVSA cocaine model of addiction. a) Schematic of the study design. **b)** Timeline of the behavioral protocol. **c)** Individual differences in number of lever presses in self-administration (SA), progressive ratio (PR) and shock-paired (Shock) sessions. **d)** Barplot showing differences in addiction index scores between high and low AI rats. **e)** Plot showing differences in mean of lever presses across ShA and LgA IVSA sessions between high and low AI rats. **f)** Barplot showing results of breakpoint analysis between high and low AI rats under ShA versus LgA. **g)** Barplot showing differences in mean of lever presses despite footshock between high and low AI rats. Error bars represent the standard error of the mean (**d-g**). Statistic represents the difference between low and high AI rats (***p < 0.001 were obtained with Two-way ANOVA in (**e)**, mixed effect model in (**f)**, and unpaired t-test in (**g)**, or using Bonferroni's multiple comparison test in **e-g**).

1383 # Figure 2

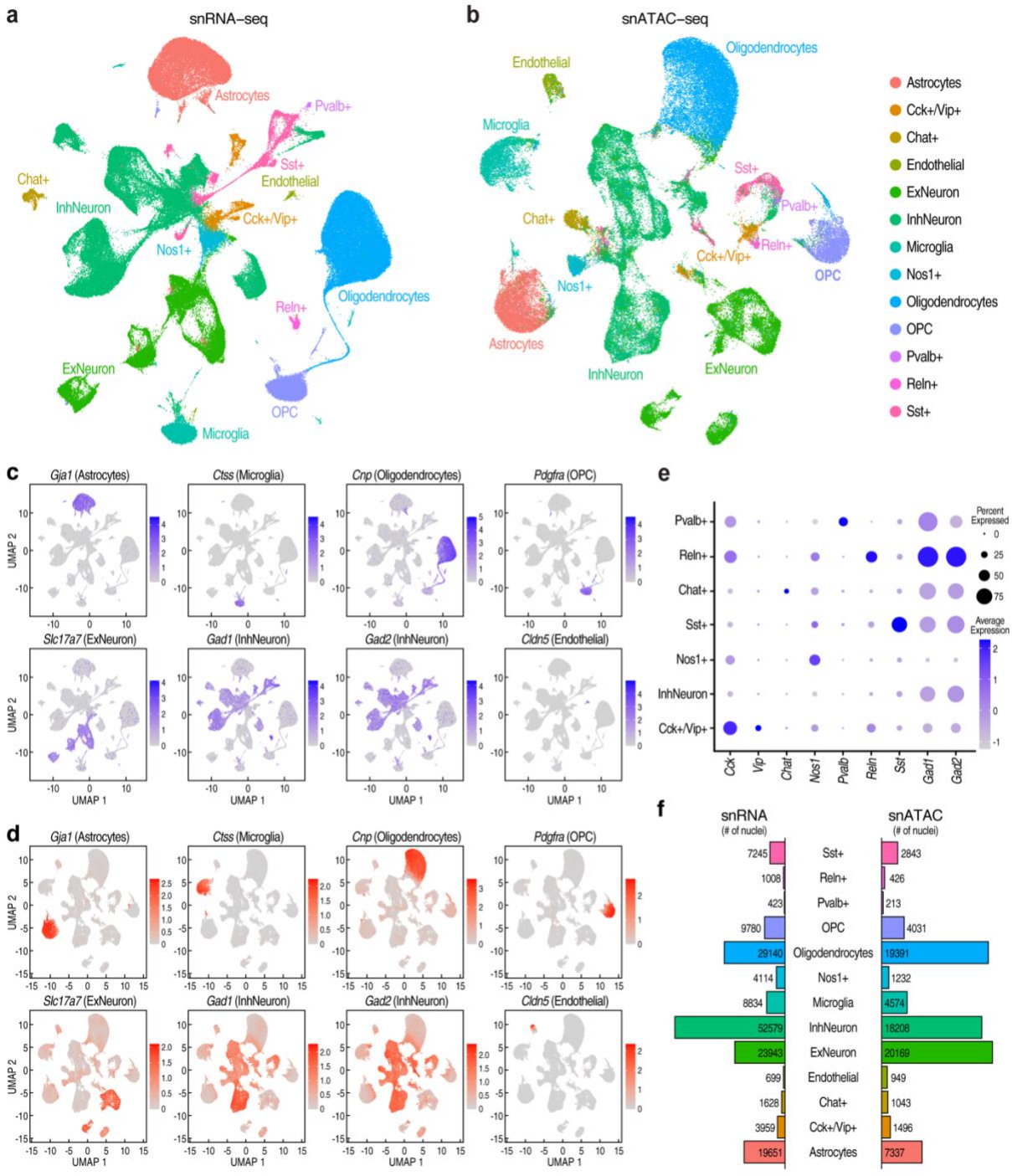

Figure 2. Summary of single nucleus RNA-seq and ATAC-seq data from the rat amygdala. a) Uniform Manifold Approximation and Projection (UMAP) plot of single nucleus RNA-seq (snRNA-seq) data from the rat amygdala. Data are combined across 19 samples, with high-, low- and -naive addiction labels. Cells are colored by cluster assignments

performed with K-nearest neighbors. We assigned cell type labels to the clusters based on the expression of known marker genes. **b)** UMAP plot of single nucleus ATAC-seq data from 12 rat amygdala samples. snATAC-seq data was integrated with the snRNA-seq data and cluster labels were transferred to the snATAC-seq cells. **c)** Feature plot showing expression of marker genes used to label major subsets of cells: *Gja1* (astrocytes), *Ctss* (microglia), Cnp (oligodendrocytes), *Pdgfra* (oligodendrocyte precursor cells (OPCs), *Slc17a7* (excitatory neurons), *Gad1* and *Gad2* (inhibitory neurons), and *Cldn5* (endothelial cells). **d)** Feature plot showing imputed gene expression of cell type-specific marker genes in snATAC-seq dataset. **e)** Expression of marker genes in cell clusters corresponding to highly specific subsets of inhibitory neurons. The shading and diameter of each circle indicate the estimated mean expression and the percentage of cells within the cluster in which the marker gene was detected. **f)** The number of nuclei assigned to each cell type cluster for the snATAC-seq and snRNA-seq datasets.

1384
1385

1386 # Figure 3

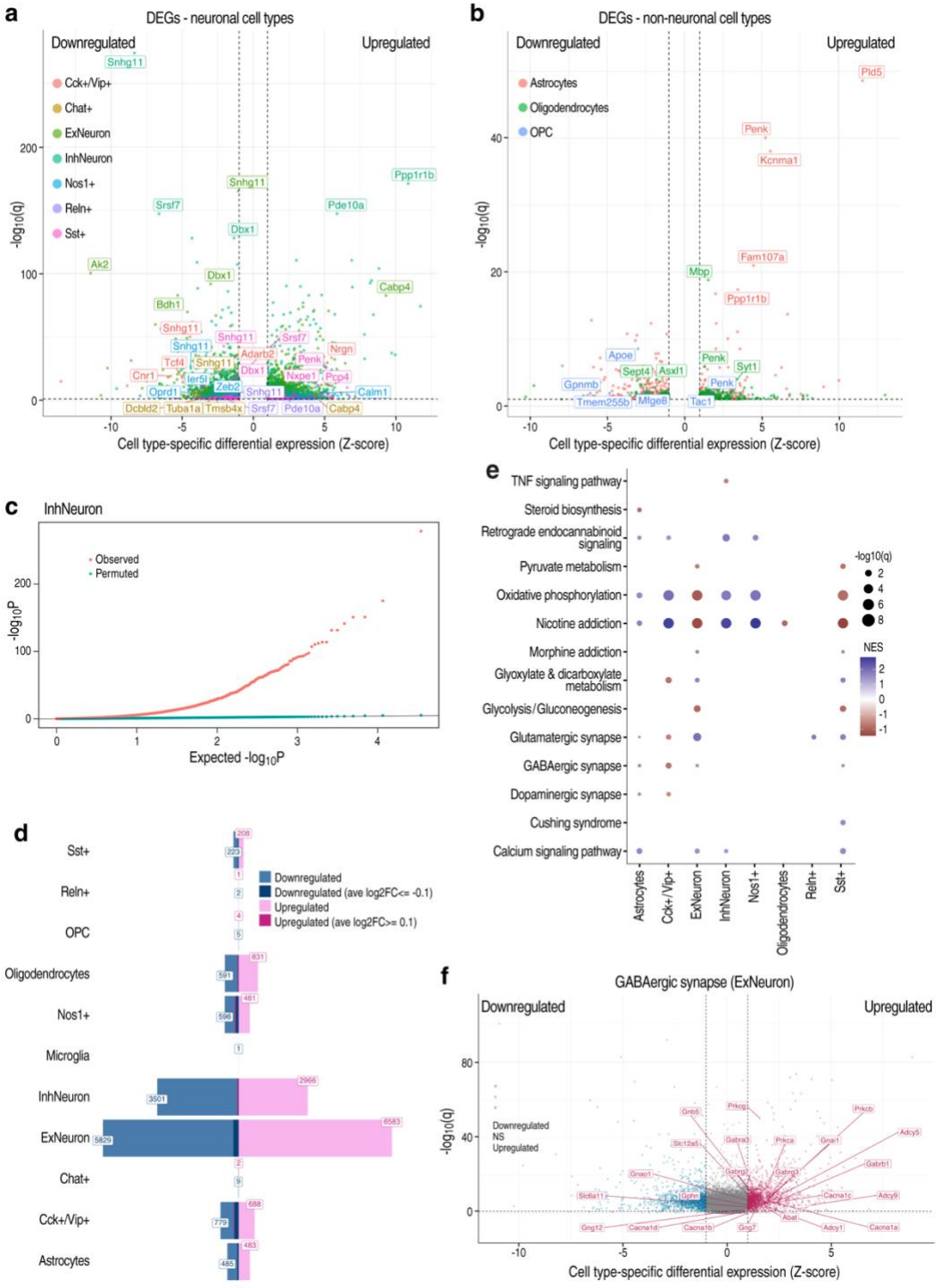

Figure 3. Differential gene expression between high and low addiction index rats. a) Volcano plot summarizing differential gene expression between high and low AI rats. Points

are colored by cell type, and the five most-significant genes for each cell type are indicated with labels. Within each cell type, we normalized the log fold changes with a z-score and plotted the cell type-specific z-scores of the log fold changes on the x-axis. The -log10 false discovery rate (FDR) corrected p-values (q-values) are plotted on the y-axis. **b)** Volcano plot summarizing differential gene expression between high and low AI rats for non-neuronal (glial) cell type clusters. **c)** Quantile-quantile plot comparing the distributions of p-values for differential gene expression tests between high and low AI rats performed in astrocytes. The x-axis is the expected -log10 p-values under the null hypothesis of no differential expression, and the y-axis is the observed -log10 differential expression p-values. P-values for differential expression were computed using MAST[60]. The blue points provide results from the same statistical test, performed after shuffling the addiction labels of the rats. **d)** Barplot showing numbers (labeled) of significant (FDR<10%) up- and downregulated DEGs by cell type. Darker shades indicate DEGs with a large foldchange (abs(avg_log2FC)≥0.1). **e)** KEGG pathways that are enriched for differentially expressed genes by cell type. **f)** Volcano plot of differential gene expression in excitatory neurons. Core enrichment genes in the glyoxalase pathway with significant differential expression are highlighted with labels.

Figure 4

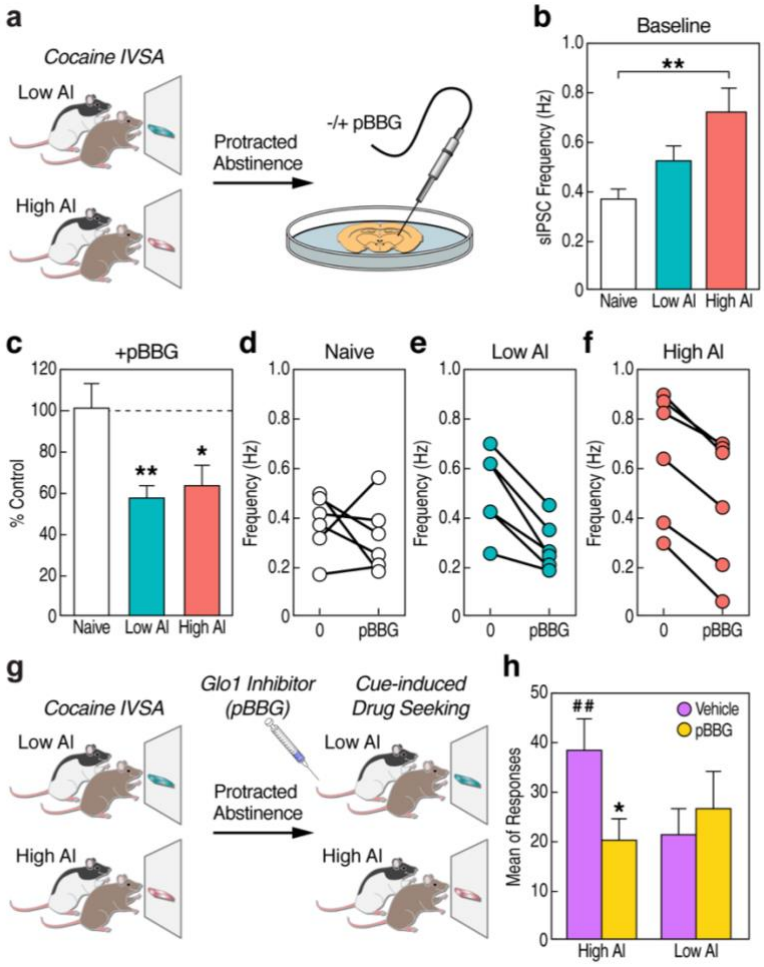

Figure 4. Electrophysiology and GLO1 inhibition experiments implicate GABAergic inhibition in cocaine addiction-like behaviors. a) Schematic showing animal model used for electrophysiology recording in the CeA. HS rats were subjected to prolonged abstinence following the same behavioral protocol used to generate the snRNA-seq and snATAC-seq data. CeA slices were harvested following this period of prolonged abstinence and treated with pBBG. Electrophysiological recordings were taken before and after pBBG treatment. **b)** Baseline iPSC frequency (measured before pBBG injection). Significant differences in the means between the three groups was observed. **c)** iPSC frequency following pBBG treatment. We observe reduced frequency in the high and low AI rats following pBBG treatment. Change in sIPSC frequency following pBBG treatment in naive (**d**), low (**e),** and high rats (**f**). **g)** Schematic of animal model used to test cocaine-seeking behavior in high and low AI rats following pBBG injection. Rats were injected with pBBG following a period of prolonged abstinence and re-exposed to the self-administration chambers in the absence of cocaine. **g)** Following injection of pBBG, high AI rats showed significantly higher cocaine-seeking behavior compared to low AI rats, which was reduced by pBBG treatment. Error bars represent the standard error of the mean (**b, c, h**). Statistic represents the difference between low and high rats (## $p<0.001$, ** $p < 0.01$, * $p<0.05$ were obtained with unpaired t-test in **(c)** and Two-way ANOVA for each measure, using Bonferroni's multiple comparison test in **c, h**).

1391 # Figure 5

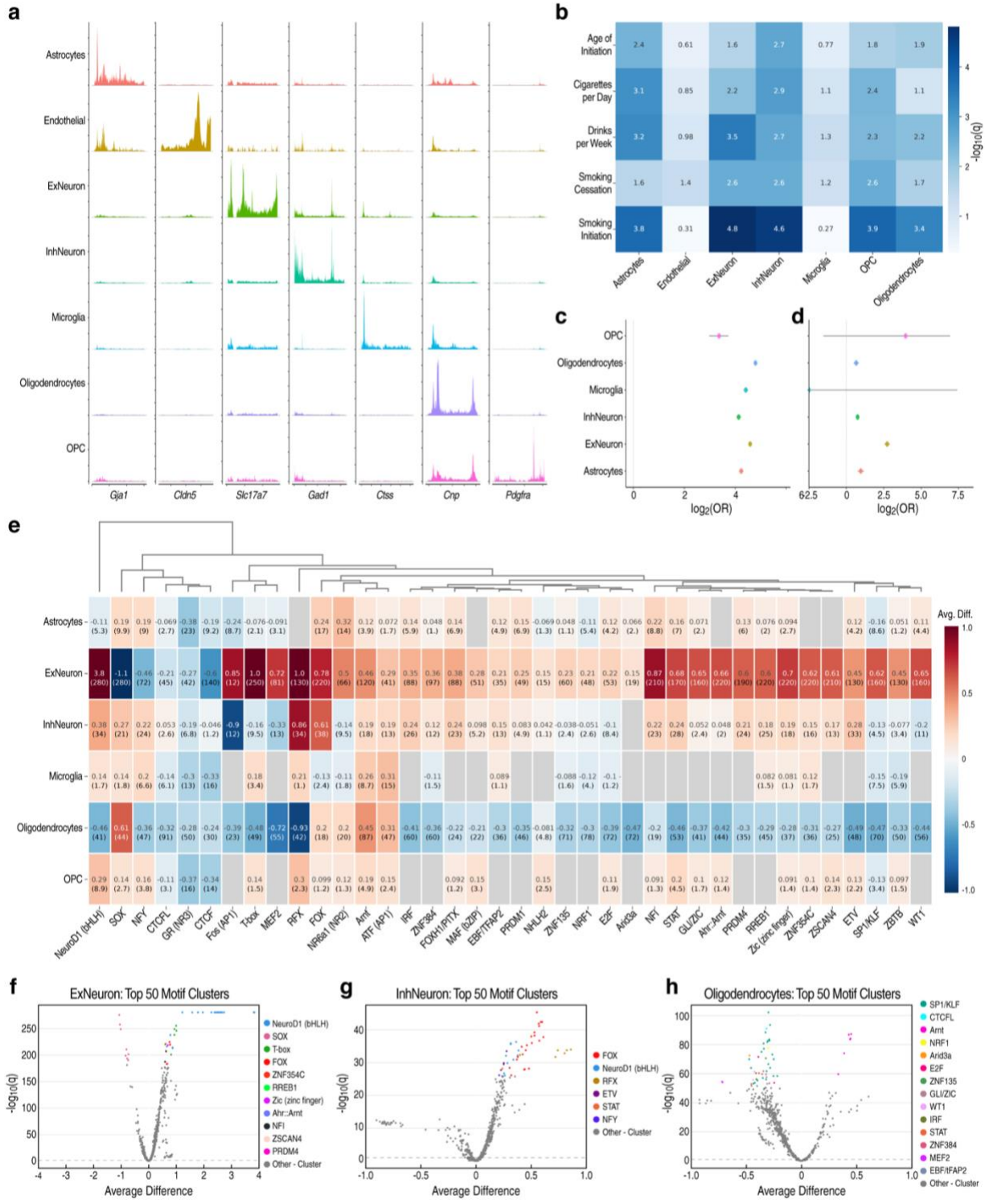

Figure 5. Analysis of chromatin accessibility and regulatory elements involved in cocaine dependence. a) Pseudobulk chromatin accessibility at the promoter regions of

marker genes for major cell types identified in our analysis. **b)** LD score regression results showing significance (-log10p) of enrichment of heritability for several traits related to alcohol and nicotine addiction in cell type-specific OCRs (mapped to hg19). **c)** Enrichment of significant DEGs for each major cell type whose promoters are also significantly differentially accessible in the snATAC-seq data. We found that all cell types tested were significantly enriched for this criterion, indicating that the findings of our snRNA-seq and snATAC-seq analyses support one another and point to long-term transcriptional changes driven by changes in accessibility of gene promoters. **d)** Enrichment of cell type specific significant differentially accessible peaks are enriched for TSS/promoter regions compared to non-differentially accessible peaks in our snATAC-seq data. This indicates that our differential analysis detects functionally relevant regulatory elements and can discriminate against genomic regions of less functional importance. **e)** Heatmap showing differential activity of various motifs in the significant differential peaks of each cell type. Values indicate average difference of chromVar deviation scores with -log10(p) in parentheses below. There are many cases where motifs display increased activity in the peaks which are more accessible in upregulated peaks in neurons while also displaying decreased activity in downregulated peaks in oligodendrocytes. **f-h)** Volcano plots showing average difference (x-axis) and -log10(q) (y-axis) of chromVAR deviation scores for top 50 motif clusters in **f)** excitatory neurons, **g)** inhibitory neurons, and **h)** oligodendrocytes.

1392

Supplementary figure legends

Figure S1. snRNA-seq profiles of 6 high AI rats. For each rat the number of unique genes detected per cell (nFeature_RNA), total number of reads within each cell (nCount_RNA), and percentage of percent mitochondrial reads are shown for each cell. Quality metrics calculated with Seurat.

Figure S2. snRNA-seq profiles of 6 low AI rats. For each rat the number of unique genes detected per cell (nFeature_RNA), total number of reads within each cell (nCount_RNA), and percentage of percent mitochondrial reads are shown for each cell. Quality metrics calculated with Seurat.

Figure S3. snRNA-seq profiles of 7 naive rats. For each rat the number of unique genes detected per cell (nFeature_RNA), total number of reads within each cell (nCount_RNA), and percentage of percent mitochondrial reads are shown for each cell. Quality metrics calculated with Seurat.

Figure S4. snATAC-seq profiles of 4 high AI rats. For each rat the ratio of mononucleosomal to nucleosome-free fragments (nucleosome_signal), percentage of fragments that fall within ATAC-seq peaks (pct_reads_in_peaks), total number of fragments in peaks (peak_region_fragments), and transcription start site enrichment score (TSS.enrichment) are shown for each cell. Quality metrics calculated with Signac.

Figure S5. snATAC-seq profiles of 4 low AI rats. For each rat the ratio of mononucleosomal to nucleosome-free fragments (nucleosome_signal), percentage of fragments that fall within ATAC-seq peaks (pct_reads_in_peaks), total number of fragments in peaks (peak_region_fragments), and transcription start site enrichment score (TSS.enrichment) are shown for each cell. Quality metrics calculated with Signac.

Figure S6. snATAC-seq profiles of 4 low naive rats. For each rat the ratio of mononucleosomal to nucleosome-free fragments (nucleosome_signal), percentage of fragments that fall within ATAC-seq peaks (pct_reads_in_peaks), total number of fragments in peaks (peak_region_fragments), and transcription start site enrichment score (TSS.enrichment) are shown for each cell. Quality metrics calculated with Signac.

Figure S7. UMAP visualization of the clusters identified in integrated single-cell data sets. (**a**) Clustering of integrated snRNA-seq dataset revealed 49 clusters. We first performed a k-nearest neighbors analysis (KNN) using the first 30 dimensions calculated by reciprocal principal component analysis (PCA). This was implemented with the FindNeighbors() function in Seurat. Next we used a modularity optimization technique using the Louvain algorithm to cluster the data, implemented with the FindClusters() function in Seurat with a resolution parameter of 0.8. (**b**) Clustering of integrated snATAC-seq data revealed 41 clusters. Latent semantic indexing (LSI) was used for dimensionality reduction rather than PCA. The first 30 dimensions minus the first dimension were used for KNN and clustering and the algorithm used for

clustering was the smart local moving (SLM) algorithm. These steps were implemented with the same Seurat functions.

Figure S8. UMAPS of snRNA-seq and snATAC-seq profiles, respectively, following batch correction of integrated datasets, grouped on: addiction index (**a, d**), rat sample (**b, e**), and batch information (**c, f**). These plots demonstrate that cells do not cluster by any of these covariates following batch correction. Integration and batch correction of the snRNA-seq dataset was performed using SCTransform while Harmony was used for the snATAC-seq dataset.

Figure S9. Feature plots showing gene activity of marker genes for each major cell type in the snATAC-seq data. Gene activity was calculated with the `GeneActivity()` function in Signac. This quantifies the number of fragments mapping anywhere within a 2kb window of an annotated gene in the genome. The gene activity information was used for integration of the snATAC-seq dataset with the snRNA-seq dataset and for imputing gene expression into the cells of the snATAC-seq dataset (see **Fig. 2d**).

Figure S10. Heatmap of top five marker gene expression within subclustered excitatory neurons.

Figure S11. QQ plots showing distribution of p-values for our differential gene expression analysis performed on our observed versus permuted data (addiction index labels associated with each cell were shuffled). MAST was the statistical test used for the analysis of both the observed and permuted datasets.

Figure S12. Venn diagram showing the number of significant DEGs (FDR<10%) that are up/downregulated with large (abs(avg_$\log_2$FC)≥0.1) or small (abs(avg_$\log_2$FC)<0.1) fold changes.

Figure S13. QQ plots showing distribution of p-values for our differential peak accessibility analysis performed on our observed versus permuted data (addiction index labels associated with each cell were shuffled). The negative binomial test was used for the analysis of both the observed and permuted datasets.

Figure S14. Bar plot showing number of significant (FDR<10%) differentially accessible peaks between high vs. low rats in each cell type.

Figure S15. Pie chart showing genomic annotations of all OCRs in our snATAC-seq dataset across all rats.

Figure S16. Histograms showing distribution of peak sizes for peaks called by MACS2 (on the BAM files for the snATAC-seq data) versus Cell Ranger's internal peak calling algorithm. MACS2 calls smaller, more precise peaks.

Figure S17. Ridge plot quantifying the number of unique fragments (log_{10}(nFrags)) per sample in the ATAC. Sample FTL_463_M757_933000320046135 was removed at this step and not included in any of our snATAC-seq due to its low number of fragments.

Supplementary tables

Table S1
List of snRNA-seq rat samples included in analysis, their addiction indexes, batch information, and Cell Ranger summary metrics.

Table S2
List of snATAC-seq rat samples included in analysis, their addiction indexes, batch information, and Cell Ranger summary metrics.

Table S3
All cell type-specific differential gene expression analysis results (MAST)

Table S4
Permutation test for differential gene expression analysis results

Table S5
KEGG GSEA results

Table S6
All cell type-specific differential peak accessibility analysis results (negbinom)

Table S7
Permutation test for differential peak accessibility analysis results

Table S8
Fisher’s exact test for enrichment of DEGs with differentially accessible promoters

Table S9
Fisher’s exact test for enrichment of differential peaks with TSS/promoter annotations